Helv Phys Acta
Vol. 65 (1992)

0018-0238/92/060767-53$1.50+0.20/0

Instability of $SU(2)$ Einstein-Yang-Mills Solitons and Non-Abelian Black Holes

Zhi-hong ZHOU[1]

Institute for Theoretical Physics, University of Zürich
Schönberggass 9, 8001 Zürich, Switzerland

Abstract

The stability of regular and black hole solutions of the $SU(2)$ spherically symmetric Einstein-Yang-Mills system is analyzed in detail. The behavior of linear radial perturbations of the system can be described by a one-dimensional, p-wave Schrödinger equation with a bounded potential. For both regular and black hole solutions, the bound states of this Schrödinger equation correspond to exponentially growing modes. The Bartnik-McKinnon solutions and the non-abelian black holes thus turn out to be unstable. We also investigate the non-linear evolutions of the perturbed solutions by solving the partial differential equations numerically. It is found that the perturbed system either collapses to a Schwarzschild black hole or explodes, depending on the details of the initial perturbations. The late time behavior of the perturbed solutions is quite universal for a sample of representative perturbations.

[1]Supported by the Swiss National Science Foundation and Dr. Tomalla Foundation.

Contents

1 Introduction

Asymptotically flat solutions of the Einstein field equations are of particular astrophysical interest. These solutions can be divided into two families: particlelike[2] and black hole solutions. We shall restrict ourselves in this work for the $SU(2)$ Einstein-Yang-Mills (EYM) system. For many years it was believed that this system has no particlelike solutions. This expectation was based on the following rigorously established facts:

1. There exist no static (or strictly stationary) gravitational solitons [1].

2. There are no static Einstein-Maxwell solitons [1].

3. No static Yang-Mills (YM) solitons exist in flat space-time [2, 3].

4. No static EYM solitons exist in 2+1 dimensions [4].

5. There are no static, spherically symmetric EYM solitons with non-vanishing electric Coulomb charges in D=3+1 [5] . The solutions with non-vanishing electric charges in D=3+1 must be singular.

6. There are no static, spherically symmetric $SU(2)$ EYM solitons with global non-vanishing magnetic charges in D=3+1 [5].

The other no-go theorems concerned with the EYM system were established by Malec [6]. However, these theorems are only valid under rather restrictive assumptions about the asymptotic behavior and the magnitude of Sobolev norms of the solutions. They do not, therefore, give any definitive conclusion about the existence of EYM solitons. In 1988, Bartnik and McKinnon (BK) discovered numerically soliton solutions of the $SU(2)$ EYM system [7]. These solutions gave for the first time strong evidence that the EYM system admits particlelike solutions.

For black hole solutions, it was generally believed that they have no 'hair'. In other words, it was expected that the structure of a stationary black hole is uniquely determined by global quantities defined at spatial infinity, such as the ADM mass, the angular momentum and the YM charges. This 'no hair' and uniqueness theorem was established rigorously only for the pure Einstein and Einstein-Maxwell (EM) systems [8, 9, 10, 11]. There have been many efforts trying to extend this theorem to include other matter models. For linear matter fields, the 'no hair' theorem probably holds, although no rigorous proof is available. However, in case of non-linear matter, it is now established by numerical examples that there is no unique answer. For EYM systems, early works showed that the black holes can not have any effective non-abelian 'hair'. In 1977, Perry constructed some particular black hole solutions for the EYM system[12]. These solutions possess Kerr-Newman metric but with Coulomb type YM connection, so they are effectively abelian. In a more general treatment, Yasskin proved that in a certain gauge any YM field with a compact symmetry group can be made parallel in the

[2]By particlelike solutions and solitons we mean in this paper globally regular and asymptotically flat solutions.

internal space so that the abelian-like solutions can be constructed from the corresponding EM solutions [13]. Since these EYM solutions are geometrically indistinguishable from the EM solutions, Yasskin then conjectured that [13] :

> The black hole solutions of the EYM systems that are stationary, asymptotically flat with a nonsingular event horizon and with gauge fields that fall off like $1/r$ at infinity and nonsingular on the horizon are essentially Kerr-Newman solutions.

This conjecture seemed to rule out the existence of the non-abelian hair. Only recently, Ershov and Gal'tsov gave a proof of the Yasskin's conjecture for the spherically symmetric $SU(2)$ EYM system with non-vanishing color magnetic charge [14]. Their so-called 'non-abelian baldness theorem' demonstrates that

> Any static spherically symmetric asymptotically flat solution of self-consistent $SU(2)$ EYM equations possessing a regular event horizon and non-zero color magnetic charge is effectively *Abelian.*

Although this 'baldness' theorem for the $SU(2)$ EYM system supports Yasskin's conjecture, it still left open the possible existence of BK-like solutions with an event horizon. The 'no hair' conjecture proposed by Yasskin in 1975 was shown to be wrong with the surprising discovery of colored black hole solutions in 1990 [15, 16, 17, 18], shortly after Bartnik and McKinnon published their particlelike solutions. These solutions provide counter examples to Yasskin's 'no hair' conjecture. Indeed, these colored black holes have vanishing global YM charges, but their metric has much richer structure than Schwarzschild metric does. The metric of these solutions is close to that of the Reissner-Nordstrøm solution outside the horizon and then approaches Schwarzschild metric at infinity.

The behavior of the BK solutions and colored black hole solutions are in many ways very similar. For instance, the basic YM field variable for all of them starts with a value between ± 1, then oscillates k times and approaches ± 1 at infinity. This behavior can be easily understood as local properties of the system. Moreover, as the horizon shrinks to zero, the exterior solution of the colored black holes converges to the BK solution, and the shooting parameters for the two families can be combined into one. Therefore, the BK solutions are *effectively* the limiting case of the colored black holes, though the boundary conditions are different for the two families. The entire solutions thus can be specified by two parameters (r_0, k), where r_0 is a continuous parameter in the interval $[0, \infty)$; $r_0 = 0$ corresponds to the regular BK solutions and $r_0 = r_h > 0$ to black hole solutions, and k is an integer denoting the number of nodes. We will discuss this issue in more detail later.

The discoveries of $SU(2)$ EYM solitons and black holes have raised many problems and attracted a lot of interest. First of all, since these solutions were established only numerically, a rigorous existence proof was needed. Such a proof was given by Smoller et al. [19] for the existence of the 'ground state' BK solution. There is, however, still no general existence proof for all BK solutions and, especially, for the colored black hole solutions. Very recently, Heusler and Straumann have derived necessary conditions of existence by extending Coleman's scaling argument to self-gravitating systems. In particular, their necessary conditions do not exclude the existence of EYM solitons and black hole solutions[20].

The other important problem concerning these solutions is their stability. Indeed, these solutions could have some astrophysical significance, provided that they would be stable. Straumann and I discovered that both the soliton solutions and the black hole solutions are unstable [21, 22]. This was, however, not immediately accepted for the black hole case. Bizon pointed out that the unstable mode which we found for the ground state black hole solution leads to a divergent YM strength field at the horizon; this is, at first sight, physically unacceptable. He thus concluded that the lowest-energy colored black hole is linearly stable [23]. This conclusion was, however, withdrawn recently in a paper by Bizon and Wald [24], because one can chose superpositions of the unstable mode and stable modes in such a way that the initial perturbation is regular at the horizon. In the long run, the unstable mode wins, of course. The colored black holes are indeed unstable. Very recently, a stability analysis based on a functional method was made for the black hole solutions [25], which confirms this conclusion.

Since both the BK and colored black hole solutions are unstable, it is interesting to investigate the evolution and final fate of these solutions under perturbations. From the physical point of view, one expects only the two possibilities: collapse or dispersion, i.e. either the perturbed field configuration collapses due to the domination of the gravity, or the configuration disperses because the repulsion of the YM field wins. In addition one may ask: if the perturbed solutions do collapse, to what will they collapse? And if it disperses, how violent is the dispersion? Obviously these questions can not be answered in the frame of linear perturbation theory. We have numerically investigated the non-linear evolutions of the perturbed BK solutions. The results of the simulations show that, depending on the details of the initial perturbation, the ground state BK solution will either collapse to a Schwarzschild black hole – rather than to a colored black hole as conjectured in ref [23] – or explode at a speed of about 3/4 of that of light [26]. Moreover, it turns out that the late time behavior of the perturbed solutions is quite universal in both cases. For instance, under a range of representative perturbations, the exploding speed for all exploding perturbations is almost the same, and the horizon forms at about same time for all collapsing perturbations, and so forth. On the other hand, since the exterior solution of the colored black holes is very close to the soliton solution, at least for a small radius of the horizon, the soliton solution can be regarded approximately as a perturbation of the colored black holes. Our numerical simulations thus also reflect the evolution of a perturbed colored black hole. Therefore, the non-linear behavior of the perturbed BK solutions provides further evidence that the colored black holes are unstable.

The existence of the BK and black hole solutions for the $SU(2)$ EYM system has encouraged people to explore higher-rank compact gauge group. There have been several works done in this direction. Recently, a general study of the non-trivial $SU(n)$ spherical symmetric EYM solutions was started by Künzle [27]. Some black hole solutions for the $SU(3)$ EYM system with specially chosed parameters were constructed numerically by Galt'sov and Volkov; the behavior of these solutions does not differ essentially from the $SU(2)$ black hole solutions [28]. Another interesting direction is to investigate non-linear σ-models. Very recently, Droz, Heusler and Straumann found numerically the soliton and black hole solutions for the $SU(2)$ Einstein-Skyrme (ES) system for a certain range of coupling constants

[29]. Some of the most interesting features of these solutions are that the ES 'stars' are at least linearly stable for certain range of coupling constants [30], and the Skyrme black holes possess 'Skyrme hair', which provides another counter example for the 'no hair' conjecture. Furthermore these new black hole solutions are presumably also at least linearly stable [31]. These researches, as well as the study of the $SU(2)$ EYM system, show that for the non-linear matter models much richer phenomena occur than one expected from all experience with the EM system. A detailed discussion on these researches is, however, beyond the scope of this paper. We shall concentrate ourselves in this paper mainly on the stability analysis for the BK and colored black hole solutions.

This paper is organized as follows. In Section 2.1, we establish necessary notations and derive the basic equations for the $SU(2)$ spherically symmetric EYM system. In Section 2.2, a proof for the non-existence of the regular $SU(2)$ EYM dyons is given. In Section 3, we discuss in detail the equilibrium configurations. Moreover, the elementary properties of the static solutions are reviewed, and the analytic solutions, the BK and colored black hole solutions are presented. In this Section proofs for the absence of regular EYM monopols and the 'non-abelian baldness' theorem as well as the derivation of the necessary conditions of existence can also be found. In Section 4, we discuss the linear stability analysis for the 'ground state' BK solutions and for the black hole solutions. In Section 5, a numerical method which includes a description of the modified MacCormack algorithm, code tests, initial and boundary conditions is given. Using this method, we simulate the nonlinear evolution of the perturbed, ground state BK solution. The numerical results are shown and discussed in this Section as well. In the final Section, we summarize all of our results presented in this paper. Proofs of some 'no go' theorems can be found in the Appendix A. A flowchart of the program we used for simulating non-linear evolution is also given in the Appendix.

Planckian units are used throughout except in the section 3.3.3 and Yang-Mills coupling constant is set equal to one.

2 The Coupled SU(2) Einstein-Yang-Mills System

In this section, we derive first the basic equations for spherically symmetric field configurations of the $SU(2)$ EYM system. Then a proof of the absence of the SU(2) dyons is presented.

2.1 Basic Equations

We consider only spherically symmetric field configurations. As long as no horizon is formed and also outside horizons, we can always introduce Schwarzschildlike coordinates for a spherically symmetric space-time. In terms of these, the metric has the form

$$g = -e^{2a}dt^2 + e^{2b}dr^2 + r^2(d\vartheta^2 + \sin^2\vartheta d\phi^2), \tag{1}$$

where a and b are only functions of r and t. With this coordinate choice the second fundamental form K_{ij} for constant time slices satisfies $K_{22} = K_{33} = 0$, which can easily be seen from the connection forms, (see, for instance, Ref [32]). In particular, the polar slicing condition $K_{22} + K_{33} = 0$ is satisfied. This slicing is most convenient to work with as long as no horizon forms.

As we are interested in spherically symmetric field configurations, we have to parametrize rotationally invariant gauge fields. In geometrical terms, one has to describe $SO(3)$ invariant connections on principle bundles (over space-time with the gauge group as the structure group). The principle bundles admit an $SO(3)$ action by bundle automophisms such that the induced action on the base manifold are the $SO(3)$ isometries of space-time[3]. Forgács and Manton have studied the same problem in less geometrical terms [35]. Without loss of generality, the general spherically symmetric ansatz for the SU(2) gauge potential can be parametrized as follows [36, 35]:

$$A = u\tau_3 dt + v\tau_3 dr + (w\tau_1 + \tilde{w}\tau_2)d\vartheta + (\cot\vartheta\tau_3 + w\tau_2 - \tilde{w}\tau_1)\sin\vartheta d\phi, \tag{2}$$

where $\tau_i (i = 1, 2, 3)$ are the Pauli matrices and u, v, w and $\tilde{w}$ depend only on r and t. The gauge freedom allows us to put $v = 0$. Furthermore, since the functions w and $\tilde{w}$ enter symmetrically in the coupled EYM system, we can choose $\tilde{w} = 0$ without loss of generality. The gauge potential can therefore be specialized to the form

$$A = u\tau_3 dt + w\tau_1 d\vartheta + (\cot\vartheta\tau_3 + w\tau_2)\sin\vartheta d\phi. \tag{3}$$

The components of the corresponding YM field become

$$\begin{aligned} F_{01} = -u'\tau_3,\ F_{02} = \dot{w}\tau_1 + uw\tau_2,\ F_{03} = \dot{w}\tau_2 - uw\tau_1, \\ F_{12} = w'\tau_1,\ F_{13} = w'\tau_2,\ F_{23} = -(1 - w^2)\tau_3, \end{aligned} \tag{4}$$

with respect to the basis of 1-forms

$$\theta^0 = dt,\ \theta^1 = dr,\ \theta^2 = d\vartheta,\ \theta^3 = \sin\vartheta d\varphi, \tag{5}$$

where the notation $' \equiv \partial_r$ and $\cdot \equiv \partial_t$ is used.

In general relativity a self-gravitating $SU(2)$ YM field system can be described by an action

$$I = \int [-R + tr(F^{\mu\nu}F_{\mu\nu})]\sqrt{-g}d^4x. \tag{6}$$

Variation with respect to the metric leads to the Einstein field equations

$$G^\mu_\nu \equiv R^\mu_\nu - \frac{1}{2}\delta^\mu_\nu R = 8\pi T^\mu_\nu, \tag{7}$$

[3]The theory of the invariant connections has been described systematically in Refs. [33]. A generalization of the representation (2) to any compact semi-simple gauge group has been developed by Brodbed and Straumann [34].

where,

$$T^{\mu}_{\nu} = \frac{1}{4\pi} tr[F^{\sigma}{}_{\nu} F_{\sigma}{}^{\mu} - \frac{1}{4}\delta^{\mu}_{\nu} F_{\alpha\beta}F^{\alpha\beta}], \tag{8}$$

and tr denotes the normalized trace, chosen such that $tr(\tau_i^2) = 1$.

With respect to the basis (5), the relevant components of the Einstein tensor are

$$\begin{aligned} G^0_0 &= -\frac{1}{r^2} + e^{-2b}(\frac{1}{r^2} - \frac{2b'}{r}), \\ G^1_1 &= -\frac{1}{r^2} + e^{-2b}(\frac{1}{r^2} + \frac{2a'}{r}), \\ G^1_0 &= \frac{2\dot{b}}{r} e^{-2b}. \end{aligned} \tag{9}$$

It is useful to introduce the following "magnetic" and "electric" quantities

$$\begin{aligned} B^2_T &= \frac{e^{-2b}}{r^2} w'^2, \; B^2_L = \frac{(1-w^2)^2}{r^4}, \\ E^2_K &= \frac{e^{-2a}}{r^2}\dot{w}^2, \; E^2_T = e^{-2(a+b)}u'^2, \; E^2_L = \frac{e^{-2a}}{r^2}u^2 w^2. \end{aligned} \tag{10}$$

In terms of (10), T^{μ}_{ν} takes the form

$$\begin{aligned} T^0_0 &= -\frac{1}{4\pi}[B^2_T + \frac{1}{2}B^2_L + E^2_K + \frac{1}{2}E^2_T + E^2_L], \\ T^1_1 &= \frac{1}{4\pi}[B^2_T - \frac{1}{2}B^2_L + E^2_K - \frac{1}{2}E^2_T + E^2_L], \\ T^1_0 &= \frac{1}{4\pi}\frac{2\dot{w}w'}{r^2} e^{-2b}, \end{aligned} \tag{11}$$

and the Lagrangian density for the YM fields becomes

$$\begin{aligned} |F|^2 &= tr(F^{\mu\nu}F_{\mu\nu}) \\ &= 4(B^2_T + \frac{1}{2}B^2_L - E^2_K - \frac{1}{2}E^2_T - E^2_L). \end{aligned} \tag{12}$$

If we define $e^{-2b} = 1 - 2m/r$ and substitute eqs. (8)–(11) into Einstein field equations (7), it follows that

$$m' = r^2[B^2_T + \frac{1}{2}B^2_L + E^2_K + \frac{1}{2}E^2_T + E^2_L], \tag{13}$$

$$a' = e^{2b}\frac{m}{r^2} + re^{2b}[B^2_T - \frac{1}{2}B^2_L + E^2_K - \frac{1}{2}E^2_T + E^2_L], \tag{14}$$

$$\dot{m} = 2e^{-2b}\dot{w}w'. \tag{15}$$

Next, we write down the YM equations $D*F = 0$ explicitly in terms of u, w, a and b:

$$\partial_t(u'e^{-a-b}) = 0, \tag{16}$$

$$\partial_t(uwe^{-a+b}) + uwe^{-a+b} = 0, \tag{17}$$

$$\partial_r(r^2u'e^{-a-b}) - 2e^{-a+b}w^2u = 0, \tag{18}$$

$$\partial_t(e^{-a+b}\dot{w}) - \partial_r(e^{a-b}w') - e^{-a+b}u^2w - \frac{e^{a+b}}{r^2}(1-w^2)w = 0. \tag{19}$$

The eqs.(13)–(19) form a complete set of equations for spherically symmetric $SU(2)$ EYM system. However, as will be proved in next section, dyon is absent for such a system. In other words, the 'electric' component u must vanish. The eqs.(13)–(19) can therefore be simplified.

2.2 Absence of the Regular SU(2) EYM Dyons

We are only concerned with solutions that are asymptotically flat, therefore we require

$$a(r) \to 0;\ b(r) \to 0;\ m(r) \to M < \infty, \text{as } r \to \infty. \tag{20}$$

From these boundary conditions, one can conclude with the help of eq.(13) that u and w have the following asymptotic behavior for large r:

$$u = u_\infty + O(\frac{1}{r}), \tag{21}$$

$$w = w_\infty + O(\frac{1}{r}), \tag{22}$$

where u_∞ in general is a function of t, which can, however, always be gauged away. Indeed, if $u_\infty \neq 0$, then a gauge transformation

$$\tilde{A} = h^{-1}Ah + h^{-1}dh \tag{23}$$

can lead to $\tilde{u}_\infty = 0$ so long as h satisfies $h = e^{\psi\tau_3}$ and ψ is chosen such that

$$u_\infty = \frac{\partial\psi}{\partial t}, \tag{24}$$

$$\frac{\partial\psi}{\partial r} = 0. \tag{25}$$

The asymptotic value w_∞ is independent of t, otherwise, m would blow up at infinity due to the term E_K^2 in eq. (13). Moreover, u must vanish for any physically interesting solution of the system (13)–(19). This can be seen as follows. Consider first an everywhere regular solution without horizons. Multiply (18) by u and then integrate from origin to infinity. This gives

$$r^2e^{-a-b}uu' \,|_0^\infty = \int_0^\infty (r^2u'^2 + 2e^{2b}w^2u^2)e^{-a-b}dr. \tag{26}$$

To keep the energy density finite, it follows from the expressions for B_L^2, E_L^2 and E_T^2 in (10) that

$$w(0) = 1; \quad u(0) = 0 \quad \text{and} \quad u'(0) < \infty. \tag{27}$$

Likewise, we have $uu' \to O(\frac{1}{r^3})$ at infinity, hence the left-hand side of (26) vanishes. As both terms in the integrand at the right-hand side of (26) are non-negative, we can conclude that either $w \equiv 0$ and $u \equiv$ const. or $u \equiv 0$. The first case brings us a singular Reissner-Nordstrøm metric, see Section 3.3.1. The only nontrivial regular solution is thus $u \equiv 0$ and $w \neq 0$. In other words, the regular solution is purely magnetic.

On the other hand, if there is a event horizon, we integrate from the horizon $r_h > 0$ to infinity, and obtain instead of (26) that

$$r^2 e^{-a-b} u u'|_{r_h}^{\infty} = \int_{r_h}^{\infty} (r^2 u'^2 + 2e^{2b} w^2 u^2) e^{-a-b} dr. \tag{28}$$

A look at the expressions for E_L^2 and E_T^2 in (10) shows that the energy density at the horizon is finite only if

$$e^{-a} u|_{r_h} < \infty \quad \text{and} \quad u'|_{r_h} < \infty. \tag{29}$$

Therefore, the left-hand side of (28) vanishes since $e^{-b(r_h)} = 0$. As before, we obtain either the Reissner-Nordstrøm solution or again $u \equiv 0$.

In summary, u vanishes identically both for the regular solutions and the colored black hole solutions. For static situations this implies in particular the theorem 5 presented in the Introduction [4]. The generalization to the time-dependent case is straightforward, because eq.(18), which is crucial in the argument of refs. [5, 14], does not involve any time derivatives.

The complete system of equations is thus simplified to

$$\frac{1}{r^2} - e^{-2b}(\frac{1}{r^2} - \frac{2b'}{r}) = 2(B_T^2 + \frac{1}{2}B_L^2 + E_K^2), \tag{30}$$

$$-\frac{1}{r^2} + e^{-2b}(\frac{1}{r^2} + \frac{2a'}{r}) = 2(B_T^2 - \frac{1}{2}B_L^2 + E_K^2), \tag{31}$$

$$\dot{b} = \frac{2}{r}\dot{w}w', \tag{32}$$

$$\partial_t(e^{-a+b}\dot{w}) - \partial_r(e^{a-b}w') - \frac{e^{a+b}}{r^2}(1-w^2)w = 0. \tag{33}$$

For latter use, here we derive two useful relations. By taking difference of eqs. (30) and (31), we obtain

$$a' - b' = \frac{e^{2b}}{r^2}(2m - \frac{(1-w^2)^2}{r}), \tag{34}$$

and addition of (30) and (31) yields

$$a' + b' = \frac{2e^{2b}}{r}(e^{-2b}w'^2 + e^{-2a}\dot{w}^2). \tag{35}$$

[4] A rigorous proof for the time-independent system can be found in ref. [37].

It is also convenient to introduce the quantity

$$\pi = e^{-a+b}\dot{w}, \tag{36}$$

and rewrite the basic equations (30)–(33) in the form

$$m' = e^{-2b}(w'^2 + \pi^2) + \frac{(1-w^2)^2}{2r^2}, \tag{37}$$

$$a' = \frac{e^{2b}}{r}(e^{-2b}(w'^2 + \pi^2) - \frac{(1-w^2)^2}{2r^2} + \frac{m}{r}), \tag{38}$$

$$\dot{m} = 2e^{a-3b}\pi w', \tag{39}$$

$$\dot{\pi} = e^{a-b}w'' + \frac{e^{a+b}}{r^2}(2m - \frac{(1-w^2)^2}{r})w' + \frac{e^{a+b}}{r^2}(1-w^2)w, \tag{40}$$

$$\dot{w} = e^{a-b}\pi. \tag{41}$$

Equation (37) is the Hamiltonian constraint. The last four equations (38)-(41) form a complete set of equations for the unknown functions m, a, w and π, and they imply that the Hamiltonian constraint propagates.

3 Static Field Configurations

In this section, after giving static equations and boundary conditions, we first demonstrate some elementary properties of the static solutions and then illustrate numerical equilibrium solutions which describe particlelike structures (gauge boson 'stars') and black holes as well as two well-known analytic solutions.

3.1 Static Equations and Boundary Conditions

For static field configurations, since all variables are time-independent, the basic equations (37)–(41) reduce to

$$m' = e^{-2b}w'^2 + \frac{(1-w^2)^2}{2r^2}, \tag{42}$$

$$a' = \frac{e^{2b}}{r}(e^{-2b}w'^2 - \frac{(1-w^2)^2}{2r^2} + \frac{m}{r}), \tag{43}$$

$$w'' = \frac{e^{2b}}{r^2}(\frac{(1-w^2)^2}{r} - 2m)w' - \frac{e^{2b}}{r^2}(1-w^2)w. \tag{44}$$

The boundary conditions are established as follows. For regular solutions we require at the origin that

$$a(0) = \text{const};\ b(0) = 0;$$
$$w(0) = 1;\ w'(0) = 0, \tag{45}$$

and hence $m(0) = 0$. On the other hand, for solutions with a regular event horizon, the boundary conditions become

$$e^{2a(r_h)} = 0, \ m(r_h) = \frac{r_h}{2}, \ w(r_h) = w_h = \text{const.} \tag{46}$$

Hence it follows from Eq.(44) that

$$w'(r_h) = \frac{(1-w_h)^2 w_h r_h}{(1-w_h^2)^2 - r_h^2}. \tag{47}$$

The conditions (45), or (46) and (47), and the requirement of asymptotic flatness (20) provide complete boundary conditions for the static field configurations.

3.2 Elementary Properties of the Static Solutions

Let us assume that w and m are smooth functions and that $e^{-2b} > 0$ on the interval $I \subset (r_0, \infty)$, where $r_0 = 0$ for regular solutions and $r_0 = r_h > 0$ for black hole solutions.

3.2.1 Nonexistence of Regular EYM Monopols

As mentioned in Section 2.2, w approaches a constant w_∞ at large r. Substitute (22) into eq. (44), we find

$$(1 - w_\infty^2) w_\infty = 0. \tag{48}$$

Therefore, w_∞ is either ± 1 or 0. However, w_∞ can not be zero, otherwise w would vanish identically. This can be seen as follows [5, 14]: multiply eq. (33) (without the terms involving time derivatives) by $(w^2 - 1)$ and integrate; it follows that

$$e^{a-b}(w^2-1)w'|_{r_0}^{\infty} = \int_{r_0}^{\infty} (2w'^2 + e^{2b} r^{-2}(w^2-1)^2) w e^{a-b} dr. \tag{49}$$

For a regular solution we have $r_0 = 0$ and $w(0) = 1$; for a black hole solution $r_0 = r_h$ and $e^{a-b} = 0$. At infinity, $w'(\infty) = 0$ for both cases. Hence, the left-hand side of (49) vanishes. If w does not change its sign in the integration interval, it is easy to see from (49) that w must be identically equal to zero or ± 1. On the other hand, if w changes sign and $w(\infty) = 0$, there must exist at least one critical point r_c where $w'(r_c) = 0$. Integrating eq. (33) from the largest critical point – in case there is more than one critical point – to infinity we find

$$e^{a-b} w'|_{r_c}^{\infty} = -\int_{r_c}^{\infty} \frac{e^{a+b}}{r^2} (1-w^2) w dr. \tag{50}$$

The left-hand side vanishes again. Since $w^2 < 1$ in the interval (r_0, ∞) (we shall prove this in next section), we have $w(r) \equiv 0$ for $r \in [r_c, \infty)$. Repeating this procedure inwards to the origin for regular solution, where $w'(0) = 0$, or to the horizon at which $e^{a-b} = 0$, we deduce $w \equiv 0$, which corresponds to the Reissner-Nordstrøm metric (see Section 3.3.1). In other words, the solution is singular and essentially abelian. Therefore, there do not exist either

regular $SU(2)$ EYM monopoles or essentially non-abelian black holes with non-vanishing magnetic charge. This proves the theorem 6 and the 'non-abelian baldness theorem' presented in the Introduction [5].

3.2.2 Necessary Conditions of Existence

Rigorous existence proofs for the BK solitons are difficult. So far only the existence of the ground state EYM soliton is proven [19]. However, very recently Heusler and Straumann generalized Coleman's scaling argument [3] to self-gravitating matter systems. With this argument they derived necessary conditions of existence for various matter systems – including the $SU(2)$ EYM system [20]. In some cases the necessary conditions exclude the existence of particle-like and black hole solutions. For the purpose of this paper, we restrict ourselves to the EYM system, although the original treatment by Heusler and Straumann is very general.

We rewrite eq. (42) in the form

$$m' = e^{-2b}U + V, \tag{51}$$

where

$$U = w'^2 \quad \text{and} \quad V = \frac{(1-w^2)^2}{r^2}. \tag{52}$$

For equilibrium configurations, the eq. (35) yields

$$\delta' = -\frac{2}{r}w'^2 = -\frac{2}{r}U \tag{53}$$

with $\delta := -(a+b)$. Hence eq.(51) becomes

$$m' = \delta' m + U + V. \tag{54}$$

From (53) and the boundary condition $\delta(\infty) = 0$, we also have

$$\delta(r) = 2\int_r^\infty \frac{U}{r}\, dr. \tag{55}$$

Therefore, m and δ are functionals of the YM variable w alone.

We discuss first particlelike solutions. The solution of the differential equation (54), satisfying $m(0) = 0$, is

$$m(r) = e^{\delta(r)}\int_0^r (U+V)e^{-\delta} dr. \tag{56}$$

In particular, the Schwarzschild mass is given by the following non-local functional of the matter field

$$M = m(\infty) = \int_0^\infty (U+V)e^{-\delta}\, dr. \tag{57}$$

[5] It is assumed that w has the asymptotic behavior (22). This assumption is somehow restrictive. For a more general proof, see [37].

The variation of M leads to correct equations of motion and therefore can be used as an action on which one can apply scaling arguments.

We choose the following radial scaling transformation for the variable w:

$$w_\lambda(r) = w(\lambda r). \tag{58}$$

The corresponding transformation for U and V are

$$U_\lambda = \lambda^2 U(\lambda r), \quad V_\lambda = \lambda^2 V(\lambda r). \tag{59}$$

Therefore we have

$$\begin{aligned} M_\lambda &= \int_0^\infty dr\,(U_\lambda + V_\lambda)e^{-\delta_\lambda} \\ &= \int_0^\infty dr\,\lambda^2(U(\lambda r) + V(\lambda r))exp(-2\lambda^2 \int_r^\infty \frac{U(\lambda r')}{r'}dr') \\ &= \int_0^\infty dr\,\lambda[U(r) + V(r)]e^{-\lambda^2\delta} \end{aligned} \tag{60}$$

For $\lambda = 1$, w is assumed to be a stationary point of the action. This means

$$\frac{dM}{d\lambda}\,|_{\lambda=1} = 0. \tag{61}$$

Thus we have

$$\int_0^\infty dr\,[U(r) + V(r)]e^{-\delta}(1 - 2\delta(r)) = 0. \tag{62}$$

From (62) we can easily see that if the space-time is 'flat', i.e. $a = b \equiv 0$, the only solution is $w \equiv \pm 1$ since $\delta \equiv 0$ and

$$U \geq 0, \quad V \geq 0. \tag{63}$$

This implies that *no* nontrivial particle-like solution can exist and, therefore, proves Coleman's theorem (theorem 3 in the Introduction, see also appendix A.2.2). On the other hand, for the self-gravitating EYM system, the scaling argument does *not* exclude the existence of particle-like solutions, provided that $1 - 2\delta(r)$ changes sign in the interval $[0, \infty)$. The particle-like solutions constructed numerically show that this necessary condition is indeed fulfilled.

A similar argument also applies to black hole solutions. Because of the presence of a horizon, we study the quantity

$$\mu(r) = m(r) - m_h, \tag{64}$$

where $m_h = m(r_h)$. Eq. (51) can be written as

$$\mu' = \delta'\mu + (1 - \frac{r_h}{r})U + V, \tag{65}$$

with the solution

$$\mu(r) = e^{\delta(r)} \int_0^r [(1 - \frac{r_h}{r})U + V]e^{-\delta(r)}\,dr. \tag{66}$$

δ is again given by eq. (53). In particular, we obtain for $\mathcal{M} := \mu(\infty) = M - m_h$ the non-local expression

$$\mathcal{M} = \int_{r_h}^{\infty} [(1 - \frac{r_h}{r})U + V] e^{-\delta(r)}\, dr. \tag{67}$$

It can be checked that this functional leads again to the correct equations of motion.

It is convenient to introduce the variable $\rho = r/r_h$ in order to fix the horizon at $\rho = 1$. Then it follows that

$$\mathcal{M} = r_h \int_1^{\infty} [(1 - \frac{1}{\rho})\tilde{U}(\rho) + \tilde{V}(\rho)] e^{-\tilde{\delta}(\rho)}\, d\rho, \tag{68}$$

where $\tilde{f}(\rho) := f(r_h\rho)$ for any function $f(r)$.

This time we make a radial scaling transformation

$$w_\lambda = w(\rho^\lambda) \tag{69}$$

for a given solution $w(\rho)$. The condition

$$\frac{d\mathcal{M}}{d\lambda}|_{\lambda=1} = 0 \tag{70}$$

leads to

$$\int_1^{\infty} \tilde{U} e^{-\delta(\rho)} [\theta(\rho) - (1 - \rho^{-1})\delta^*(\rho)]\, d\rho = \int_1^{\infty} \tilde{V} e^{-\delta(\rho)} [\gamma(\rho) + \delta^*(\rho)]\, d\rho, \tag{71}$$

with

$$\begin{aligned} \theta(\rho) &= 1 + \ln\rho - (1 + 2\ln\rho)/\rho, \\ \gamma(\rho) &= 1 - \ln\rho, \end{aligned} \tag{72}$$

and

$$\delta^* = 2\int_\rho^{\infty} \frac{\tilde{U}(\rho')}{\rho'}(1 + 2\ln\rho')\, d\rho'. \tag{73}$$

Although this necessary condition is not as simple as (62) for regular solutions, it does not exclude the existence of colored black hole solutions.

3.2.3 Local Analysis of Static Solutions

It is obvious from the eqs. (42)–(44) that the static $SU(2)$ EYM system is invariant under the transformation $w \to -w$, and as the right-hand side of (42) is non-negative, m is a monotonic function of r.

On the interval I, the function $w(r)$ takes values only in the strip $(-1, 1)$, i.e. $|w| < 1$ for $r > r_0$. To see this, we consider two cases, namely, $|w(r_c)| \neq 1$ and $|w(r_c)| > 1$ for a critical point $r_c > r_0$. At critical points of w, Eq. (44) shows that

$$r^2 e^{-2b} w w'' = -(1 - w^2)w^2. \tag{74}$$

Hence, if $|w(r_c)| = 1$, the second order of derivative vanishes, and so do all other higher-order derivatives, according to Eq.(44). The only solution is $|w| \equiv 1$ and $m = \text{const}$, which corresponds to the Schwarzschild solution (see Section 3.3.1). Thus we have to consider only the cases $|w(r_c)| \neq 1$. For $| w(r_c) | > 1$, it follows from Eq.(74) that

$$ww'' > 0, \tag{75}$$

which means that there is *no* maximum (minimum) for $w(r_c) > 1$ ($w(r_c) < -1$). However, if $w(r)$ had crossed 1 (-1) somewhere at $r^* > r_0$, and return to 1 (-1) at infinity to fulfill asymptotic flatness, then there would exist a maximum (minimum) between r^* and infinity with $w(r_c) > 1$ ($w(r_c) < -1$). This contradiction prevents w from leaving the strip $(-1, 1)$. Note that for $|w(r_c)| < 1$ Eq.(74) gives $ww'' < 0$. This implies that the critical points of w are maxima (minima) if $0 < w(r_c) < 1$ ($0 > w(r_c) > -1$); w can oscillate within the strip $(-1, 1)$.

In summary, a regular solution has to start with the values given by (45) (see Section 3.3.2 for details), and a non-abelian black hole solution must start with the values determined by (46) and (47) (see Section 3.3.3). Both of them may oscillate between ± 1 and must asymptotically approach ± 1 at infinity. Only recently, the existence of such a solution was proved rigorously by Smoller at al. [19]; these authors showed that the 'ground state' regular solution exists. However proof of existence of the 'exited state' solutions and, especially, black hole solutions is still absent.

3.3 Equilibrium Solutions

3.3.1 Analytic Solutions

There are two well-known analytic solutions for the equations (42)–(44). In one case we have $w \equiv \pm 1$ and

$$\begin{aligned} m &= M = \text{const}, \\ e^{2a} &= e^{-2b} = 1 - \tfrac{2M}{r}, \end{aligned} \tag{76}$$

where M is the total mass. The solution (76) represents the Schwarzschild metric with vanishing YM curvature if $M > 0$, or Minkowski metric if M is chosen to vanish.

The other analytic solution is

$$\begin{aligned} w &\equiv 0, \; m = M - \frac{1}{2r}, \\ e^{2a} &= e^{-2b} = 1 - \frac{2M}{r} + \frac{1}{r^2}, \end{aligned} \tag{77}$$

which is just the Reissner-Nordstrøm metric with magnetic charge $g = 1$ and $u(1)$-valued YM curvature (so effectively abelian)

$$F = (\frac{w}{r^2}\theta^1 \wedge \theta^2 + \theta^2 \wedge \theta^3)\tau_3. \tag{78}$$

Both solutions are, of course, singular at the origin $r = 0$.

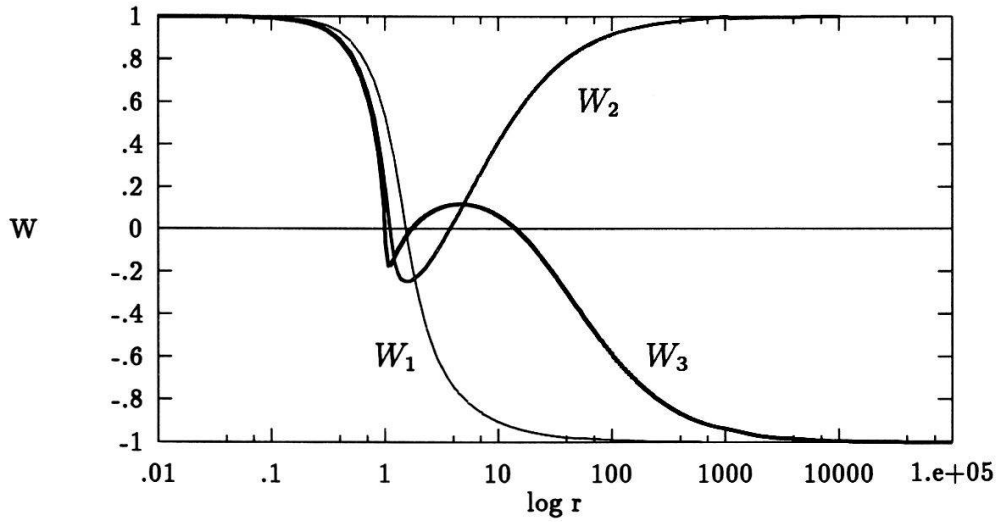

Figure 1: The variable w of the Yang-Mills field for the first three Bartnik–McKinnon solutions. The subscript of w denotes the number of zeros in $[0, \infty)$.

3.3.2 Regular Particlelike Solutions

To find regular solutions from (42)–(44), we require the energy density to be finite at $r = 0$. This implies

$$w = 1 - \beta r^2 + O(r^4),$$
$$m = 2\beta^2 r^3 + O(r^5), \ for\ r \to 0. \tag{79}$$

This condition, together with the asymptotic flatness requirement (20), reduces the problem of finding regular solutions of (42)–(44) to a regular two-point boundary value problem. By adjusting carefully the free parameter β to 'shoot' the boundary values, a discrete family of regular solutions was found by Bartnik and McKinnon [7]. We have repeated their calculations and arrived at the same results. The first three solutions are plotted in Fig.1. Some interesting features are observed with these results, for instance:

- For each solution w_k, where k stands for the number of zeroes of w, there are three distinguished regions: an inner core region with $r < 1$,$w \sim 1$,a transition region: $r > 1$, $w \sim 0$, in which the metric is close to Reissner-Nørdstron, and finally an outer-region, $r \gg 1$, $w \sim \pm 1$, where the metric approaches the Schwarzschild metric with total mass M_k.

- The global YM charge are all equal to zero.

- The total mass for each solution can be indexed by an integer k, the number of zeros. The sequence of masses M_k increases monotonically and approaches 1 as $k \to \infty$. An

empirical mass formula is given by[6]

$$M_k = 1 - 1.05944e^{-1.8095k}. \tag{80}$$

- The shooting parameters β_k seem to converge to 0.7065, as $k \to \infty$.
- The zeros of the solutions w_k accumulate near $r = 1$.
- B_T^2, B_L^2, and hence the energy density T_{00} fall off rapidly for $r > 1$.

As already mentioned in the Introduction, these regular solutions came as a surprise, since various no-go theorems for related systems lead to the expectation that such solutions should not exist. In Section 4 we shall present in detail a linear stability analysis for these solutions. It turns out that the BK solutions are unstable [21]. For this reason, the physical interest of the BK solutions is less clear.

3.3.3 Black Hole Solutions

The static $SU(2)$ EYM system (42)–(44) admits also a family of black hole solutions [15, 16, 17, 18]. These solutions can be constructed in the following steps:

1. Suppose there exists a horizon r_h where $2m(r_h) = r_h$. From eqs (42) and (44) we obtain the first derivatives

$$\begin{aligned} w_h' &= \frac{(1-w_h^2)w_h r_h}{(1-w_h^2)^2 - r_h^2}, \\ m_h' &= \frac{(1-w_h^2)^2}{2r_h^2}, \end{aligned} \tag{81}$$

   where the subscript h stands for r_h.

2. Pick a value r_h, and calculate m, w at $r = r_h + \epsilon$ using the Taylor expansion

$$\begin{aligned} m(r) &= \frac{r_h}{2} + m_h'\epsilon + O(\epsilon^2), \\ w(r) &= w_h + w_h'\epsilon + O(\epsilon^2) \end{aligned} \tag{82}$$

   and (81). Therefore, $m(r)$ and $w(r)$ are determined uniquely by the parameter w_h that replaces β in Section 3.3.2 as a shooting parameter. The expansions (82) help us start the integration at $r_h + \epsilon$ rather than at r_h in order to avoid the coordinate singularity.

3. Shoot for asymptotically flat solutions by adjusting the parameter w_h.

[6]The formula for M_k given in ref.[7] is wrong.

Following these steps we have repeated and confirmed the numerical calculations published in the refs. [15, 16, 17, 18]. The first two solutions with the horizon at $r_h = 1$ can be found in Fig.2. These numerical results show that although the global YM charges and the angular momentums of these solutions vanish, their metric is much richer than Schwarzschild. Therefore, the existence of such black hole solutions is in contradiction with 'no hair' conjecture.

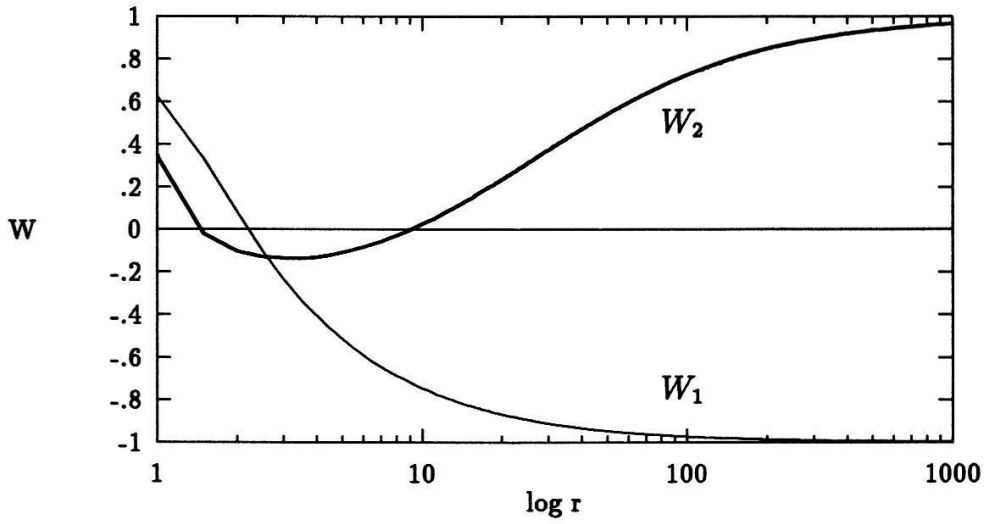

Figure 2: The first two non-abelian black hole solutions with the horizon located at $r_h = 1$.

Unlike the regular solutions, the black hole solutions are specified by two parameters r_h and k, the radius of the event horizon and the number of zeros of w, respectively. For a fixed horizon $r_h \in (0, \infty)$, the black hole solutions form a discrete sequence which can be indexed by the integer k. The total mass of the solution in the sequence increases monotonically as k increases and converges to a finite value. If $r_h \geq 1$ (remember that we are using planckian units), the limiting solution coincides with the Reissner-Nordstrøm solution as $k \to \infty$, and the limiting mass converges to $M = r_h/2 + 1/2r_h$ [28]. It is easy to see that for $r_h \to \infty$ and $k \to \infty$, the limiting mass approaches that of the Schwarzschild solution, i.e. $r_h/2$. Finally, if $r_h < 1$, the limiting mass is independent on r_h and converges to 1 from below as $k \to \infty$ [28].

The black hole solutions have a similar structure for all values of $r_h \in (0, \infty)$. For instance, w starts at the value w_h, then oscillates k times around zero and approaches asymptotically ± 1. These common structures suggest that there is certain symmetry hidden behind these solutions [18]. Such a symmetry indeed exists. This is because of a well-known scaling property of the EYM system [3, 7]. In order to see this, we introduce the variable

$$x = \frac{r}{r_h} \tag{83}$$

and rewrite the basic eqs.(30), (31) and (33) for equilibrium configurations as follows

$$\frac{1}{x^2} - e^{-2b}\left(\frac{1}{x^2} - \frac{2b'}{x}\right) = \frac{2\kappa}{r_h^2}\left(B_T^2(x) + \frac{1}{2}B_L^2(x)\right), \tag{84}$$

$$-\frac{1}{x^2}+e^{-2b}(\frac{1}{x^2}+\frac{2a'}{x})=\frac{2\kappa}{r_h^2}(B_T^2(x)-\frac{1}{2}B_L^2(x)), \tag{85}$$

$$\partial_x(e^{a-b}w')+\frac{e^{a+b}}{x^2}(1-w^2)w=0, \tag{86}$$

where $\kappa=4\pi G$ has been restored and primes denote derivatives with respect to x. Therefore, the dependence of the black hole solutions on r_h can be absorbed in the effective coupling constant

$$\tilde{G}=\frac{G}{r_h^2}. \tag{87}$$

Apart from the common properties for all r_h, the black hole solutions with $r_h >> 1$ and $r_h << 1$ have their own characteristics. For $r_h >> 1$, the effective coupling constant $\tilde{G}\to 0$. Then, eqs. (84)–(86) read

$$\frac{1}{x^2}-e^{-2b}(\frac{1}{x^2}-\frac{2b'}{x})=0, \tag{88}$$

$$-\frac{1}{x^2}+e^{-2b}(\frac{1}{x^2}+\frac{2a'}{x})=0, \tag{89}$$

$$\partial_x(e^{a-b}w')+\frac{e^{a+b}}{x^2}(1-w^2)w=0. \tag{90}$$

Eqs. (88) and (89) are just Einstein equations in vacuum, and eq.(90) describes a YM field on a fixed background satisfying with (88) and (89). This result is not surprising because the YM field and gravitational field are decoupled when $\tilde{G}\to 0$. Apply scaling argument described in section (3.2.2) to this case, we find the necessary condition (71) reduces to

$$\int_1^\infty \tilde{U}\theta(\rho)\,d\rho=\int_1^\infty \tilde{V}\gamma(\rho)\,d\rho. \tag{91}$$

By checking (72), one can convince oneself that the existence of nontrivial solutions is not excluded by the necessary condition. It is already known that there exists indeed an analytic, $k=1$ YM solution on a Schwarzschild background [38], that is

$$w(x)=\frac{x-(3+\sqrt{3})/2}{x+3(1+\sqrt{3})/2}. \tag{92}$$

Thus it is natural to expect that the $k=1$ black hole solutions should approach asymptotically the solution (92) as $r_h\to\infty$. The numerical calculations show that this is just the case [28].

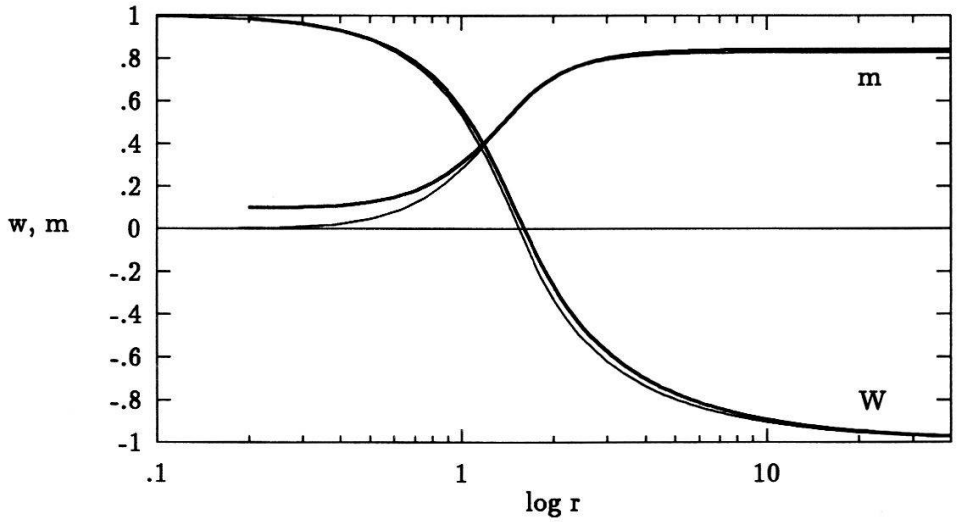

Figure 3: The BK ground state solutions, w and m (thin lines), and a non-abelian black hole solution (bold lines) with the horizon located at $r_h = 0.2$.

For the opposite case, $r_h << 1$, the exterior solution of the colored black holes converges to the BK solution despite of the different boundary conditions. This can be seen from Fig.3 where a black hole solution with $r_h = 0.2$ is depicted. This was observed numerically by Galt'sov and Volkov [15, 16, 28] [7]. We have also independently investigated this question. We found that the two shooting parameters β in (79) for the regular solutions and w_h for the black hole solutions can be transformed into each other when $r_h \to 0$. To see this, let us expand w and m around the horizon to second and third order, respectively:

$$\begin{aligned} w(r) &= w_h + w_h'(r - r_h) + \frac{w_h''}{2}(r - r_h)^2 + O(\epsilon^3), \\ m(r) &= m_h + m_h'(r - r_h) + \frac{m_h''}{2}(r - r_h)^2 + \frac{m_h'''}{6}(r - r_h)^3 + O(\epsilon^4). \end{aligned} \tag{93}$$

The first derivatives are given by (81). By differentiating both sides of the eqs.(42) and (44), we can get all higher order derivatives. For instance, differentiating eq.(44) leads to

$$w_h'' = -\frac{4(1 - w_h^2)w_h w_h' + r_h^{-1}(1 - w_h^2)^2 + 2r_h m_h' + r_h(1 - 3w_h^2)}{r_h^2(1 - 2m_h') - (1 - w_h^2)^2 + 2r_h m_h} w_h', \tag{94}$$

and so on. It is easy to see that all orders of the derivative are uniquely determined by w_h. Next, we require that the energy density at the horizon is finite for any r_h. This implies that

$$w_h = 1 - cr_h^2 + O(r_h^3), \tag{95}$$

[7] Volkov and Galt'sov misinterpreted their numerical results in refs. [15, 16]. This confusion was caused by the wrong formula for M_k—see (80) and footnote there—given in Ref.[7].

Table 1: Shooting parameters w_h of the 1-node black hole solutions for different r_h. The parameter c is calculated from $c = (1 - w_h)/r_h^2$.

r_h	0.4	0.2	0.1	0.01
w_h	0.933137	0.982636	0.995561	0.9999547
c	0.4179	0.4341	0.4439	0.4529

where c is an arbitrary constant. Therefore, for $r_h \to 0$, it follows from (81) that

$$w_h' = -2cr_h + O(r_h^3), \tag{96}$$

$$m_h' = 2c^2 r_h^2 + O(r_h^4). \tag{97}$$

Likewise, we have

$$w_h'' = -2c + O(r_h^2), \tag{98}$$

$$m_h'' = 8c^2 r_h + O(r_h^3), \tag{99}$$

and

$$m_h''' = 12c^2 + O(r_h^2). \tag{100}$$

If $r_h = 0$, these derivatives become

$$w_h = 1,\ w_h'' = -2c, \text{ and } m_h''' = 12c^2 \tag{101}$$

and

$$w_h' = m_h' = m_h'' = 0. \tag{102}$$

The expansion (93) then reduces to

$$w(r) = 1 - cr^2, \tag{103}$$

$$m(r) = 2c^2 r^3. \tag{104}$$

Now it is clear that the constant c is nothing but the shooting parameter β for the regular solutions. The expansion can be rewritten as

$$w_h = 1 - \beta r_h^2 + O(r_h^3). \tag{105}$$

We have shifted the 1-node black hole solution from $r_h = 0.4$ to $r_h = 0.01$ and calculated c, using eq.(95). The results are shown in Table 1. From there we can see that as $r_h \to 0$, c approaches 0.4537 — the shooting parameter for the 1-node BK regular solutions. We have also shifted 2-node and 3-node black hole solutions to $r_h = 0.01$. The values of c converge again to the shooting parameters for the corresponding regular solutions. Thus (105) holds

indeed. With the help of eq.(105), the two independent shooting parameters are combined into one.

The whole spherically symmetric solutions of the $SU(2)$ EYM systems can be specified by two parameters (r_0, k), where $r_0 \in [0, \infty)$ is a continuous parameter and $k = 0, 1, 2, \cdots$. The parameter $r_0 = 0$ corresponds to the BK solutions and $r_0 = r_h > 0$ to the black hole solutions. The integer $k > 0$ denotes the number of the zeros and $k = 0$ corresponds to the Reissner-Nordstrøm solution. However, it is worth indicating that the BK solution is not the limiting case of the black hole solution since the boundary conditions of e^{-2b} are different for the two families. Indeed, as long as the horizon r_h is set to vanish, the metric e^{-2b} jumps from zero to one. the limiting process is thus discontinuous. But, on the other hand, when $r_h \to 0$ the exterior solution of the black holes does approach the BK solution in the sense of the two families can not be distinguished globally. This can be seen from Fig.4, where we plot e^{-2b} for the BK solution and for the black hole solutions with different r_h, and also from Fig.3. Therefore we may regard the BK solution as *effectively* limiting case of the black hole solutions despite of different boundary conditions.

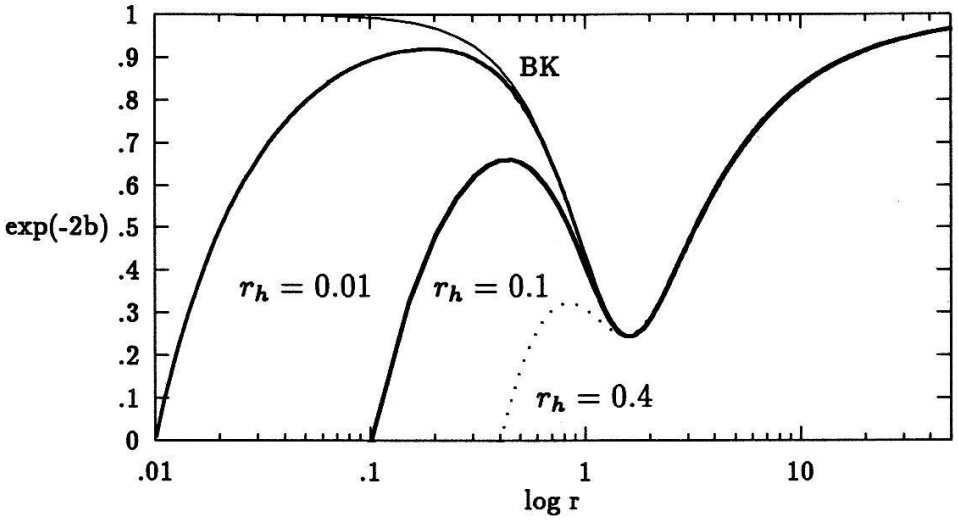

Figure 4: The profiles of metric e^{-2b} for the 1-node BK solution (thin line) and 1-node black hole solutions with different horizons (bold and dotted lines). The boundary values are different for the two families.

As already mentioned, the discovery of these non-abelian black hole solutions is surprising since it is in contradiction with the 'no hair' conjecture. However linear stability analysis as well as non-linear numerical computations show that these solutions are unstable too. We shall analyze the stability of these colored black holes in next section and in section 5.

4 Analysis of Linear Stability

In view of the "principle of linear stability", it suffices to consider only spherically symmetric perturbations, provided that the system turns out to be unstable. This is indeed the case

for the BK particlelike solutions. For the black hole solutions, although the conclusion is the same, analysis of linear stability is not as simple because the event horizon is involved.

4.1 Linear Perturbation Equations

For a small-amplitude, spherically symmetric departures from a static equilibrium configuration, described by $a_e(r)$, $b_e(r)$ and $w_e(r)$, we introduce the notation

$$\begin{aligned} a(r,t) &= a_e(r) + \delta a(r,t), \\ b(r,t) &= b_e(r) + \delta b(r,t), \\ w(r,t) &= w_e(r) + \delta w(r,t), \end{aligned} \tag{106}$$

where δa, δb and δw are considered to be small quantities. Relative to the basis (5), the linear deviations of the relevant components of the Einstein tensor $G^{(1)}_{\mu\nu}$ are given by (see, e.g., ref.[32])

$$G_0^{0(1)} = -\frac{2}{r}(\delta b' - 2b_e'\delta b + \frac{\delta b}{r})e^{-2b_e}, \tag{107}$$

$$G_1^{1(1)} = \frac{2}{r}(\delta a' - 2a_e'\delta b - \frac{\delta b}{r})e^{-2b_e}, \tag{108}$$

$$G_0^{1(1)} = \frac{2}{r}e^{-2b_e}\dot{\delta b}. \tag{109}$$

Linear deviations of the components of the energy-momentum tensor become

$$T_0^{0(1)} = -\frac{1}{4\pi r^2}(2e^{-2b_e}(w_e'\delta w' - w_e'^2\delta b) - \frac{2}{r^2}(1-w_e^2)w_e\delta w) \tag{110}$$

$$T_1^{1(1)} = \frac{1}{4\pi r^2}(2e^{-2b_e}(w_e'\delta w' - w_e'^2\delta b) + \frac{2}{r^2}(1-w_e^2)w_e\delta w) \tag{111}$$

$$T_0^{1(1)} = \frac{1}{4\pi r^2}2\dot{\delta w}w_e'e^{-2b_e}. \tag{112}$$

From the tr Einstein equation $G_0^{1(1)} = 8\pi T_0^{1(1)}$, it follows that

$$\dot{\delta b} = \frac{2}{r}w_e'\dot{\delta w}. \tag{113}$$

It has a solution

$$\delta b = \frac{2}{r}w_e'\delta w + f(r), \tag{114}$$

where $f(r)$ is a free function of r. On the other hand, the tt Einstein equation $G_0^{0(1)} = 8\pi T_0^{0(1)}$ reads

$$\delta b' = (2b_e - \frac{1}{r})\delta b + \frac{2}{r}(w_e'\delta w - w_e'^2\delta b) - \frac{2}{r^2}(1-w_e^2)w_e\delta w. \tag{115}$$

Substitute the solution (114) into (115), with the help of the static equations, we find

$$f' = 0. \tag{116}$$

Thus f has to be a constant. We require that $\delta b \to 0$ and $\delta w \to 0$ at infinity. This implies

$$f(r) \equiv 0. \tag{117}$$

Finally the sum of tt and rr Einstein equations $G_0^{0(1)} + G_1^{1(1)} = 8\pi(T_0^{0(1)} + T_1^{1(1)})$ provides the relation

$$\delta a' - \delta b' = \frac{4}{r^3} e^{2b_e}(1 - w_e^2) w_e \delta w + 2(\frac{1}{r} + a_e' - b_e')\delta b. \tag{118}$$

The linearization of the Yang-Mills equation $D * F = 0$ about the equilibrium solution gives, after straightforward calculations, the following differential equation for δw:

$$\begin{aligned} & e^{-2(a_e - b_e)} \ddot{\delta w} - \delta w'' - (a_e' - b_e')\delta w' - (\delta a' - \delta b') w_e' \\ & - \frac{2}{r^2} e^{2b_e}(1 - w_e^2) w_e \delta b - \frac{1}{r^2} e^{2b_e}(1 - 3w_e^2)\delta w = 0. \end{aligned} \tag{119}$$

The only metric perturbations which enter the linearized equation (119) are δb and $\delta a' - \delta b'$. It is amazing to see that with (114) and (118) these perturbations are already determined by δw, without any further integration. This fact simplifies the analysis very much.

In order to study the stability of the system, we decompose δw into

$$\delta w(r, t) = \xi(r) \exp(i\sigma t), \tag{120}$$

and then substitute (114) and (118) into (119). We obtain the pulsation equation

$$-\xi'' + \frac{1}{2}\alpha' \xi' + U\xi = \sigma^2 e^{\alpha} \xi, \tag{121}$$

where, we have introduced the notation $\alpha = -2(a_e - b_e)$ and the effective potential

$$U = \frac{4}{r}(w_e')^2 (\frac{\alpha'}{2} - \frac{1}{r}) - \frac{8}{r^3} e^{2b_e} w_e w_e' (1 - w_e^2) - \frac{1}{r^2} e^{2b_e}(1 - 3w_e^2). \tag{122}$$

It is easy to see that $U - 2/r^2$ is bounded on $[0, \infty)$.

4.2 Small Deviation from the BK Solutions

4.2.1 Instability of the BK Solutions

The pulsation equation (121) is an eigenvalue equation. According to the theory of linear stability, the configuration is stable against arbitrary small radial perturbations if and only if all eigenvalues σ^2 are positive (see, e.g. [39]). Physically we require finite energy density everywhere. This implies $\xi(r) = \kappa r^2$ as $r \to 0$, where κ is an irrelevant constant because of the linearity of the eq. (121). We further impose a boundary condition $\xi(r) \to 0$ as $r \to \infty$.

It is very helpful to bring (121) into the form of a standard radial Schrödinger equation. For this we introduce a new radial coordinate ρ defined by

$$\frac{d\rho}{dr} = e^{[\alpha(r)-\alpha(0)]/2}, \quad \rho(0) = 0. \tag{123}$$

The perturbation equation (121) then has the form of an one-dimensional, p-wave Schrödinger equation:

$$[-\frac{d^2}{d\rho^2} + \frac{2}{\rho^2} + V(\rho)]\xi(\rho) = E\xi(\rho), \tag{124}$$

where

$$E = \sigma^2 e^{\alpha(0)},$$
$$V(\rho) = U(\rho)e^{-[\alpha(\rho)-\alpha(0)]} - \frac{2}{\rho^2}. \tag{125}$$

The potential $V(\rho)$ is illustrated in Fig.5. It is not difficult to show that V is bounded for all ρ, this is the reason that the term $2/\rho^2$ s introduced in eq. (124).

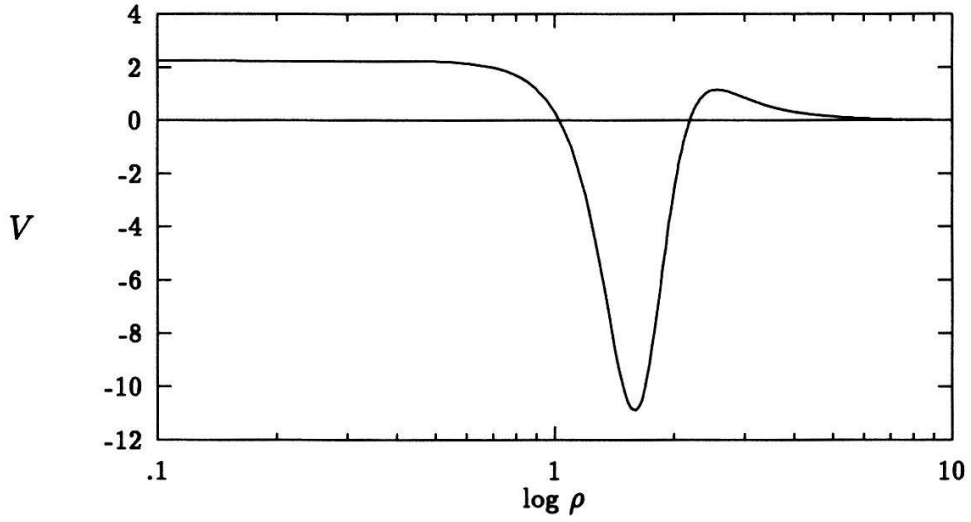

Figure 5: The bounded effective potential V.

The existence of a bound state is demonstrated numerically. The eq. (124) is integrated along with eqs. (42)–(44)by using the D02EJF routine from the NAG mathematical library. The equilibrium solutions of the eqs. (42)–(44) are used to generate the potential V in Schrödinger equation (124). With tolerance 10^{-12}, we found a bound state for 1-node BK solution, which is shown in Fig.6 as a function of original radial coordinate r [21]. The corresponding eigenvalue σ^2 is

$$\sigma^2 = -0.0525. \tag{126}$$

The perturbation δw grows unboundedly due to the negative sign of σ^2. The BK solution is thus *linearly unstable*. General theorems then imply that the BK solution is also unstable in the sense of Liapunov. One may ask what the final fate is for the perturbed solutions if they are unstable. This will be the subject of the section 5.

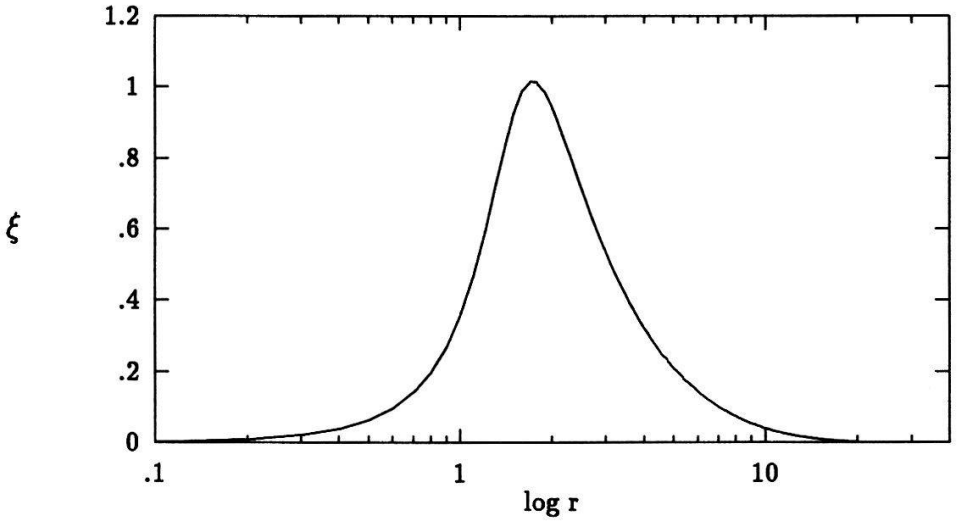

Figure 6: A bound state with eigenvalue $\sigma^2 = -0.0525$ for the linearly perturbed, 1-node solution.

4.2.2 Determination of the Bound States

It is interesting to ask if there are other bound states. The well-known Bargmann bound [40] for the number of (p-wave) bound states gives a rather loose upper limit 5. However, since the potential $V(\rho)$ in the p-wave Schrödinger eq. (124) satisfies

$$\lim_{\rho\to\infty}[\rho^2 V(\rho)] = 0, \tag{127}$$

we can use the well-established 'variable phase method' in quantum scattering theory to compute the number of bound states (see, e.g. [41]). Maison has found with this method that the number of bound states is equal to the number of zeros of BK solutions [42]. In the following we shall give a brief description of this method.

Introduce a 'phase shift function' δ_l, which is governed by a first-order differential equation [41]:

$$\delta_l'(\rho) = -k^{-1}V(\rho)[\cos\delta_l(\rho)\hat{j}_l(k\rho) - \sin\delta_l(\rho)\hat{n}_l(k\rho)]^2 \tag{128}$$

with initial condition

$$\delta_l(0) = 0, \tag{129}$$

where $\hat{j}_l$ and $\hat{n}_l$ are Riccati-Bessel functions. For p-waves ($l = 1$), these functions have form

$$\hat{j}_1(x) = -\cos x + \frac{\sin x}{x};\ \hat{n}_1(x) = -\sin x - \frac{\cos x}{x}. \tag{130}$$

The well-known Levinson theorem states that the zero-energy value of the phase shift δ_l is π times N_l, the number of the bound states with angular momentum l (see, e.g. ref.[41]), i.e.

$$N_l\pi = \delta_l \mid_{k=0} . \tag{131}$$

One can not, however, compute $\delta_k(\rho)$ directly for $k = 0$ since eq. (128) is singular at $k = 0$. The value of phase shift at $k = 0$ is actually defined by continuity from the values for $k \neq 0$. By solving (128) and (129) for small k, we computed the phase shift function δ_1. The potential V in eq. (128) is again generated by the equilibrium BK solutions. The result for the ground state BK solution is depicted in Fig.7a. Fig.7a shows that δ_1 converges to a step function with a $mod(\pi)$ jumping as $k \to 0$. According to Levinson's theorem, there is exactly one bound state for the ground state BK solution. Therefore the bound state which we found numerically in the last section is unique.

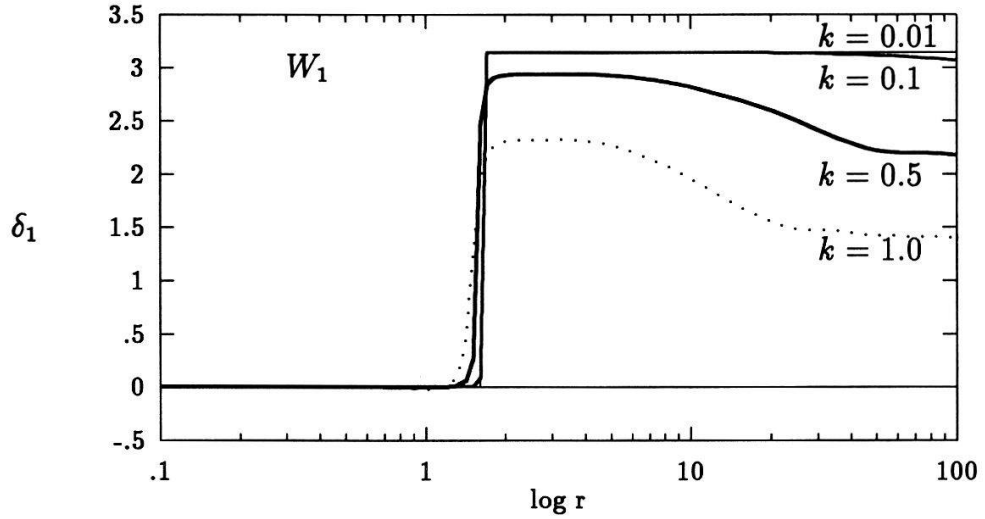

Figure 7a: The P-wave phase shift function δ_1 for the potential V belonging to the 1-node solution. As $k \to 0$, the phase shift function converges to π. One concludes from Levinson's theorem that there exists exactly one bound state.

We have also calculated the phase shifts for 2-node and 3-node BK solutions. The results, depicted in Fig.7b, demonstrate that the phase shift for w_2 is 2π and for w_3 is 3π. This means that there exist two and three bound states for 2-node and 3-node solutions, respectively. These results confirm Maison's conclusion: the number of bound state is equal to the number of zeros.

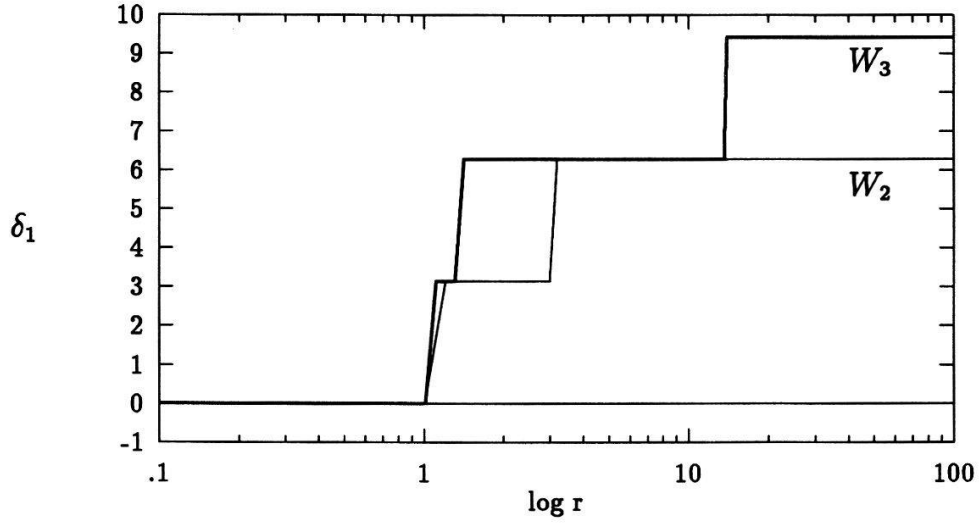

Figure 7b: The P-wave phase shift functions δ_1 for the potential V with 2-node (thin line) and 3-node (bold line) solutions. In both cases $k = 0.01$. According to the Levinson's theorem, the number of bound state is equal to the number of nodes.

4.3 Instability of Non-Abelian Black Holes

To analyze the stability of black hole solutions, we first carry out a linear stability analysis along the same lines as for the BK solutions. Instead of (123), which is no longer a good definition because of the existence of the horizon, we introduce a new radial coordinate ρ by

$$\frac{d\rho}{dr} = e^{\alpha/2}, \quad \rho(r_h) = -\infty. \tag{132}$$

It follows that the amplitude $\xi(\rho)$ for linear perturbations satisfies the eigenvalue equation

$$(-\frac{d^2}{d\rho^2} + U(\rho)e^{-\alpha})\xi(\rho) = \sigma^2\xi(\rho). \tag{133}$$

Eqs. (42)–(44) and (133) form a complete set of equations. For black hole solutions, the boundary conditions are $\xi(r) \to 0$ for $r \to r_h$ as well as for $r \to \infty$. Without loss of generality (see discussion in section 3.3.3), r_h can be set to 1. With the same method as in section 4.2.1), we found numerically a zero-node eigenfunction of (133) with a negative σ^2 [22]

$$\sigma^2 = -0.02685. \tag{134}$$

This describes an exponentially growing mode. The effective potential $Ue^{-\alpha}$ in (133) vanishes asymptotically as $\rho \to -\infty$. Therefore, from eq. (133), we obtain the asymptotic behavior

$$\xi \sim e^{\omega\rho}; \ \rho \to -\infty \tag{135}$$

where $\omega^2 = -\sigma^2$ and $\omega > 0$.

In order to check whether such a bound state is well-behaved at the horizon, we transform to Kruskal coordinates

$$\begin{aligned} u &= e^{\eta\rho}\cosh(\eta t), \\ v &= e^{\eta\rho}\sinh(\eta t), \end{aligned} \tag{136}$$

where η has to be chosen as

$$\begin{aligned} \eta &= \frac{1}{2}\frac{d}{dr}(e^{-\alpha/2})|_{r_h} \\ &= \frac{1}{2r_h}[1 - \frac{(1-w_e^2(r_h))^2}{r_h^2}]e^{a(r_h)+b(r_h)}. \end{aligned} \tag{137}$$

It is obvious that the amplitude ξ transforms like a scalar (since ϑ and φ remain unchanged). This implies that ξ, as a function of the Kruskal coordinates, is certainly bounded at the horizon.

The metric perturbations transform as

$$\delta g^K_{\alpha\beta} = \frac{dx^\mu_S}{dx^\alpha_K}\frac{dx^\nu_S}{dx^\beta_K}\delta g^S_{\mu\nu}, \tag{138}$$

where K and S refers to Kruskal and Schwarzschild, respectively. It is also easy to see that all metric perturbations in Kruskal coordinates (and, by construction, the background metric) remain finite as the horizon is approached. For instance,

$$\begin{aligned} \delta g^K_{uu} &= (\frac{dt}{du})^2\delta g^S_{tt} + (\frac{d\rho}{du})^2\delta g^S_{\rho\rho} \\ &= \eta^{-2}e^{-4\eta\rho}(\delta g^S_{tt}v^2 + \delta g^S_{\rho\rho}u^2) \\ &= -\delta g^S_{tt}\eta^{-2}e^{-2\eta\rho} \\ &= -2\delta a e^{2a_e}\eta^{-2}e^{-2\eta\rho}. \end{aligned} \tag{139}$$

It follows from (118) and (34) that

$$\delta a' - \delta b' \sim e^{2b_e}\xi + \xi \tag{140}$$

where we have used the solution (114)

$$\delta b \sim \xi. \tag{141}$$

In the ρ-coordinate, we have

$$\partial_\rho(\delta a - \delta b) \sim \xi \to 0 \tag{142}$$

as $\rho \to -\infty$. Hence, $\delta a \to const.$ The metric perturbation δg^K_{uu} is therefore bounded at the horizon, and so is δg^K_{vv}. These well-behaved perturbations, $\delta\xi$, δa and δb, led us to reach the

conclusion in ref. [22]. However, Bizon pointed out that the perturbed YM field strength behaves like [23]

$$\begin{aligned} \delta F &= (\dot{\delta w} dt + \delta w' dr) \wedge \Omega \\ &= \eta^{-1} \omega \xi e^{-\eta\rho} (du + dv) \wedge \Omega \\ &\sim e^{(\omega-\eta)\rho}, \end{aligned} \tag{143}$$

where $\Omega = \tau_1\theta^2 + \tau_2\theta^3$. For the ground state ($k = 1$) black hole solution, $\sigma^2 = -0.02685$, we have

$$\omega = 0.164 \quad \text{and} \quad \eta = 0.184, \tag{144}$$

it follows that $\omega - \eta < 0$, thus δF blows up as $\rho \to -\infty$. From this, Bizon concluded that the 1-node non-abelian black hole solution is linearly stable [23]. This is, however, not the case, as was noted later by Bizon and Wald [24]. Indeed, we can choose superpositions of the unstable mode with the stable modes in such a way that the initial perturbation of F is regular. In the long run, the unstable mode will win. The colored black hole turns out to be unstable.

In next section, we shall discuss non-linear evolutions of the perturbed EYM system. As we shall see, the results coincide with the linear analysis.

5 Nonlinear Perturbation

In this section, we shall study numerically non-linear evolutions of the perturbed equilibrium configurations of the EYM system. This section is based on ref. [26], but in more detail.

5.1 Numerical Method

5.1.1 Algorithm

The basic nonlinear partial differential equations (37)–(41) were solved with the help of a modified MacCormack predictor-corrector scheme [43, 44, 45]. We recall that the standard MacCormack algorithm for an equation of the type $\partial_t U(t,x) = F(U, \partial_x U, ...)$ proceeds along the following scheme. For the time slice $n+1$, the 'predicted' value of U, U_p^{n+1}, is defined by

$$U_p^{n+1} = U^n + \Delta t F(U^n, \partial_+^{(2)} U^n, ...), \tag{145}$$

where U^n are the values of U on the nth time slice and $\partial_+^{(2)}$ is a forward 2-point difference

$$\partial_+^{(2)} U^n(x_i) = \frac{U^n(x_i + \Delta x) - U^n(x_i)}{\Delta x}. \tag{146}$$

The "corrected" value of U on the time slice $n+1$ is then given by

$$U^{n+1} = \frac{1}{2}[U_p^{n+1} + U^n + \Delta t F(U_p^{n+1}, \partial_-^{(2)} U_p^{n+1}, ...)], \tag{147}$$

where $\partial_-^{(2)}$ is a backward 2-point difference,

$$\partial_-^{(2)}U(x_i) = (U(x_i) - U(x_i - \Delta x))/\Delta x. \tag{148}$$

An alternative method is to backward difference at the predictor level and forward difference the corrector equation. Second derivatives are always centered differenced, that is

$$\partial^2 U(x_i) = \frac{U(x_i + \Delta x) - 2U(x_i) + U(x_i - \Delta x)}{\Delta x^2}. \tag{149}$$

Although the two steps in above MacCormack algorithm may be unstable separately, the overall combined scheme is stable and of second order in space and time due to the cancellations of the truncation errors of each step.

Instead of $\partial_\pm^{(2)}$, we used in a modified scheme 4-point difference formulae for the first spatial derivatives (see, e.g. [46]),

$$\partial_\pm^{(4)}U(x_i) = \pm\frac{-2U(x_i \mp \Delta x) - 3U(x_i) + 6U(x_i \pm \Delta x) - U(x_i \pm 2\Delta x)}{6\Delta x}. \tag{150}$$

The second derivatives are still approximated by centered differencing. This modified MacCormack algorithm has shown better performance in numerical computations of the bosonic star [45].

The strategy for solving (37)–(41) involves the following steps. First one gives initial values for w and π. With the help of (37) and (38) we can then compute the initial data for m and a. In a predictor loop, eqs. (39), (40) and (41) provide predicted values for m, π and w. For instance,

$$m_p^{n+1} = m^n + \Delta t(2e^{a-3b}\pi w')^n. \tag{151}$$

The predicted values a_p^{n+1} for a is obtained by integrating eq. (38) inward from the outer edge of the spatial grid to the origin, using the predicted values of m, w and π. Next the corrector loop 'corrects' these three quantities. For example, the m in eq. (151) is then updated to

$$m^{n+1} = \frac{1}{2}[m_p^{n+1} + m^n + \Delta t(2e^{a_p - 3b_p}\pi_p w_p')^{n+1}]. \tag{152}$$

The corrected value for a is obtained by another inward integration of (38). This spatial integration is performed using a fourth order Runge-Kutta method. The data at the midpoint between grid points required by this method are obtained by cubic spline interpolations provided by the E01BAF and E02BBF routines from the NAG mathematical library. We programmed these steps; a flowchart of the program we used can be found in Appendix B.

Both the grid size and time steps are equally spaced. The working values which were chosen are $\Delta r = 0.008$, $\Delta t = 0.001$ (thus $\Delta t \ll \Delta r$). The radial range of our grid covers $[0.01, 40]$, which is a compromise of CPU time and accuracy.

Table 2: Parameters in (153), (154) for the simulations shown in the figures.

simulations	$\bar{r}$	σ	k
$I_1^{\pm}$, $II_1^{\pm}$	1.5	5.0	0.1
I_2^{-}, $II_2^{\pm}$	2.0	5.0	0.1
I_2^{+}	2.0	5.0	0.2

5.1.2 Initial and Boundary Conditions

We chose two different types of perturbation as initial conditions. In the first class we only perturb w from its ground equilibrium configuration w_e and set $\pi = 0$ (hence $E_K = 0$). In the second class w is taken to be in w_e, but π and thus the kinetic energy density of the YM fields are nonvanishing. For both cases, Gaussian-like perturbations are added in some region of the equilibrium configuration. The region, height and width of the perturbation can be chosen at will. Once the perturbation has been made, we can compute the corresponding initial metric functions m and a using eqs. (37)–(38) with appropriate boundary conditions. From the asymptotic form of m for large distances we obtain the total mass M, which is in general different from that of the unperturbed equilibrium configuration.

In a representative sample of the initial perturbations, we distinguish four classes of initial conditions for the YM field variables w and π as follows:

$$\begin{aligned} \textit{type } I^{\pm}: \quad & w = w_e \pm k\ exp[-\sigma(r-\bar{r})^2], \\ & \pi = 0; \end{aligned} \tag{153}$$

$$\begin{aligned} \textit{type } II^{\pm}: \quad & w = w_e, \\ & \pi = \pm k\ exp[-\sigma(r-\bar{r})^2]. \end{aligned} \tag{154}$$

The values of the positive parameters $\bar{r}$, σ, k, which we chosed in the simulations discussed below, are listed in Table 2.

Beside the initial conditions we must also supply boundary conditions at the origin and at the outer boundary of the grid. Like for equilibrium configurations, the desired regular solutions of the time-dependent system can also be expanded in powers of r near the origin. Similarly, the basic differential equations (37)–(41) lead to certain relations for the coefficients of these expansions. As a result of the requirements of finite energy density and regular metric, we have the following expansions for m and w near the origin,

$$\begin{aligned} w &= 1 - \beta r^2 + O(r^4), \\ m &= 2\beta^2 r^3 + O(r^5), \end{aligned} \tag{155}$$

which have the same form as (79), but here β can be a function of t. The initial value of β is fixed by the initial condition for w and is arbitrary. Its time dependence is determined

by the evolution. (For the equilibrium solution β is the 'shooting parameter'.) With the help of (155), we can start integrating at $r_0 = 0.01$, rather than at $r_0 = 0$. (Note that the eqs. (37)–(41) are singular at $r = 0$.) The expansion (155) provides also the boundary value of w at r_0, which are required by the derivatives of w in eqs. (39) and (40). The boundary value $w(r_0)$ is chosen as

$$w(r_0) = 1 + (\frac{r_0}{r_0 + \triangle})^2 (w(r_0 + \triangle) - 1), \tag{156}$$

where $\triangle$ denotes the spatial step. The β, therefore, does not appear explicitly.

At the outer boundary one should impose a kind of outgoing-wave condition. We have, however, fixed the functions w and π to their initial values. This means that outgoing waves are not allowed to escape the grid. It turns out, however, that – for the size of our grid – the interesting phase of the evolution of the perturbations occurs well before the outgoing wave hits the boundary. This holds particularly for the collapsing perturbations. The boundary value of the lapse e^{2a} can be fixed at will because of the freedom of choosing the time variable. In our code, a is always normalized such that $a(r \to \infty) = 0$. The value of m at the outer boundary is determined by the evolution. We use eq. (39) to evolve m on interior points of the grid and then use the Hamiltonian constraint (37) to check its consistency.

5.1.3 Code Tests

A first obvious test is to run the program by chosing the unperturbed BK ground state solution as an initial condition. Because of the intrinsic instability of the solution, small numerical truncation errors accumulate and are magnified at long times. We found little deviation from the equilibrium solution for times $t \leq 24$. In this time interval the maximal deviations for e^a, m, w are about 0.2%, 0.06%, and 0.6%, respectively. From the linear stability analysis of Section 4.2.1 we know that the intrinsic time scale for instabilities is 4.4, as $|\sigma^2| = 0.0525$. The time interval $t = 24$ is thus about 5.5 times longer than this intrinsic time scale. Therefore these numerical deviations are acceptable. Moreover, we also observed that for smaller spatial and temporal steps the numerical stability can maintain longer than $t = 24$. On the other hand, as a matter of the fact, it will turn out that even small perturbations of the equilibrium configuration have already reached the nonlinear regime at shorter times.

Another very useful check is provided by the Hamiltonian constraint. As eqs. (38)–(41) form a complete set of equations for all unknown variables, the Hamiltonian constraint (37) therefore performs as an independent monitor of the accuracy. We found in our simulations that this constraint was satisfied to a high accuracy, better than 10^{-5}. However, if the perturbed solution collapses to a black hole, the Hamiltonian constraint fails to maintain the accuracy of 10^{-5} around the Schwarzschild radius; the Hamiltonian at the radius, $H(r_h)$, can become as high as 10^{-2} at $t = 24$ for the simulation I_1^-. After $t = 24$, the simulation is no longer reliable since the Hamiltonian constraint is no more satisfied. In Fig.8a, absolute values of the Hamiltonian constraints at $r = 1.0$, $1.66(r_h)$ and 2.0 for the simulation I_1^- are plotted against time, from which we can see that the deviation of the Hamiltonian constraint from zero rises drastically around the Schwarzschild radius while it is still below 10^{-5} in other

Table 3: Comparison of the simulations I_1^- for different spatial and temporal steps, but constant ratio $\Delta r/\Delta t$. The value $r = 1.66$ is the Schwarzschild radius for the parameters of I_1^-.

t	Δr (10^{-3})	r=1.0		r=1.66		r=5.0	
		w	π	w	π	w	π
0		0.5099	0.0	-0.1906	0.0	-0.7960	0.0
24	8	0.4696	-0.2139	-1.0312	-1.5493	-1.0577	0.0135
	4	0.4696	-0.2138	-1.0312	-1.5929	-1.0577	0.0135

regions. In Fig.8a, we also show the Hamiltonian constraint at the Schwarzschild radius when the spatial step size is chosen to be one half of the previous simulation. The Hamiltonian constraint for the simulation I_1^+ at different times is presented in Fig.8b.

In order to check the consistency of the results, we have varied the temporal step Δt and the spatial step Δr. Instead of our working temporal step $\Delta t = 1.0 \times 10^{-3}$, we also tested $\Delta t = 0.5 \times 10^{-3}$. It turned out that the resulting differences for w and π never become larger than 10^{-4} for $t < 30$. The working spatial step $\Delta r = 8.0 \times 10^{-3}$ was also taken two times smaller. In Table 3, we compare the simulations I_1^- that lead to collapse (see Section 5.2) for different spatial and temporal steps. The spatial step was changed from 8×10^{-3} to 4×10^{-3}, meanwhile, the temporal step was shortened by one half so that the ratio $\Delta r/\Delta t$ was kept constant. From the table we can see that the results are quite independent of the chosen parameters.

As an another check, we applied the program to study the collapse of textures and compared our results with the analytic solutions published in refs. [47, 48]. Furthermore, we also compared our MacCormack code with the code used in ref. [49]. In both cases we got agreement to a high accuracy.

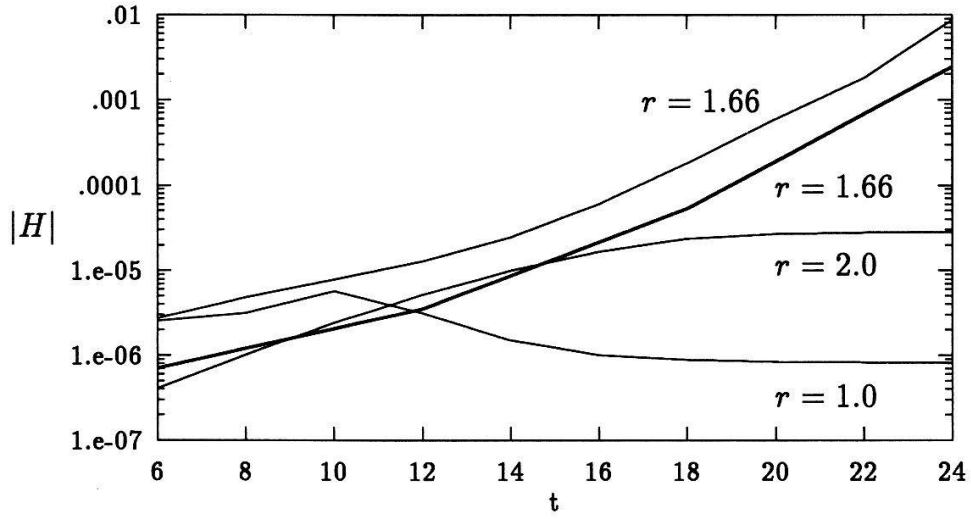

Figure 8a: The absolute value of the Hamiltonian constraint vs. time for simulation I_1^- for different spatial steps. The constraint is broken at the Schwarzschild radius when the event horizon is formed. While, the Hamiltonian constraint is satisfied within 10^{-5}. The bold line corresponds to the simulation with the same parameters chosen as for the thin lines but for half spatial step size. The broken Hamiltonian constraint at the horizon indicates that the simulation is no longer reliable after $t = 24$.

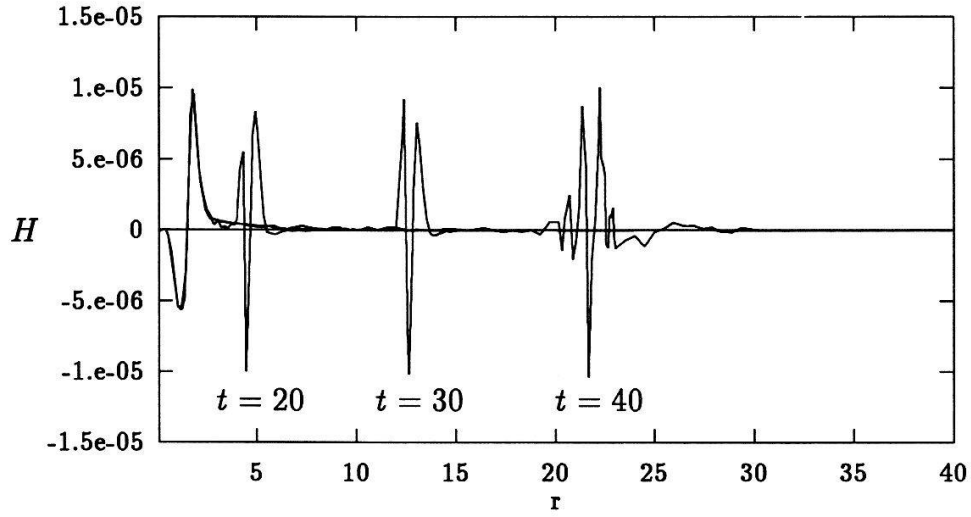

Figure 8b: The Hamiltonian constraints for simulation I_1^+ are plotted at different times.

5.2 Results and Discussions

In this section we present and discuss our numerical results for evolutions of the perturbed, ground state BK solution. Our program was run on an Alliant computer.

In the simulation I_1^-, the parameters are chosen such that the initial perturbation is concentrated inside the Schwarzschild radius which corresponds to the total mass of the system (Fig.9). For this perturbation gravity wins and the gauge boson star collapses. Figs. 10a – 10d present the evolution of various quantities for the parameters I_1^- in Table 2. Fig.10a shows the radial profile of the field amplitude w at various times. Snapshots are taken in time intervals $\Delta t = 4$. The star collapses rapidly to a Schwarzschild black hole since outside $r = 1.64$ the value of w becomes close to -1, which corresponds to the Schwarzschild metric (see Section (3.3.1)). This can also be clearly seen from Fig.10b, where the evolution of the metric variable m is depicted. At $r_h = 1.642$, $2m/r_h$ approaches 1 from below as the perturbation evolves. At $t = 24$, the ratio of $2m/r_h$ is about 0.998, which indicates that an event horizon is forming. Outside the horizon the mass function becomes constant, which is just another characteristic of the Schwarzschild black hole. The lapse function e^a, whose evolution is plotted in Fig.10c, is very small ($< 10^{-5}$) at $t = 24$. This reflects the well-known fact that Schwarzschild-like coordinates are inappropriate when the star becomes almost a black hole. At late times, the variable π, which is proportional to $\dot{w}$, becomes strongly peaked near the horizon (Fig.10d). The appearance of the horizon and the strong peak of π at $t = 24$ suggest that the numerical results are no more reliable for t larger than about 24.

In the simulation I_1^-, the total initial mass is (in Planckian units) equal to 0.8297, which is slightly larger than the ground state mass 0.8286 of the BK solution. The mass of the formed black hole is 0.8194, which means that about 1.2% of the total initial mass is lost during collapse.

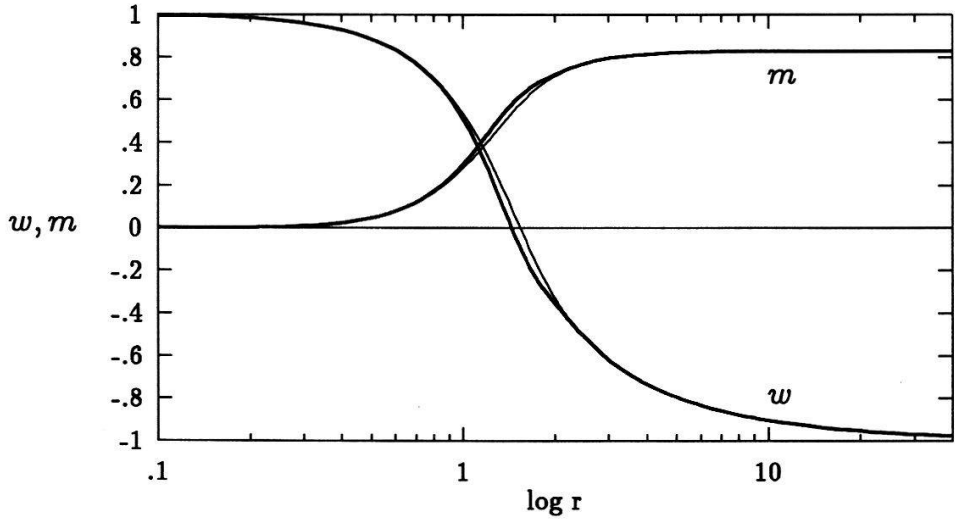

Figure 9: Initial perturbations of the YM amplitude w and the metric function m for simulation I_1^- (bold lines). The thin lines depict the equilibrium BK ground state solution.

For the parameters I_1^+ (sign change in (153)) the star expands very rapidly, as can be seen from Figs.11a – 11d. In this case the repulsion of YM fields wins. Notice that the outgoing motion has not yet reached the boundary of the grid at $t = 40$. From Fig.11b we can see that the 90% mass boundary moves outwards with about 3/4 of the speed of light. The explosion of the star is also reflected in the evolution of the lapse function (Fig.11c) and in the outward motion of the peak of π shown in Fig.11d. Like for I_1^-, the parameters in I_1^+ are chosen such that the initial perturbation is still concentrated inside the Schwarzschild radius. This is changed in the runs $I_2^\pm$ for which the position of the gaussian-like initial perturbation was placed outside the Schwarzschild radius.

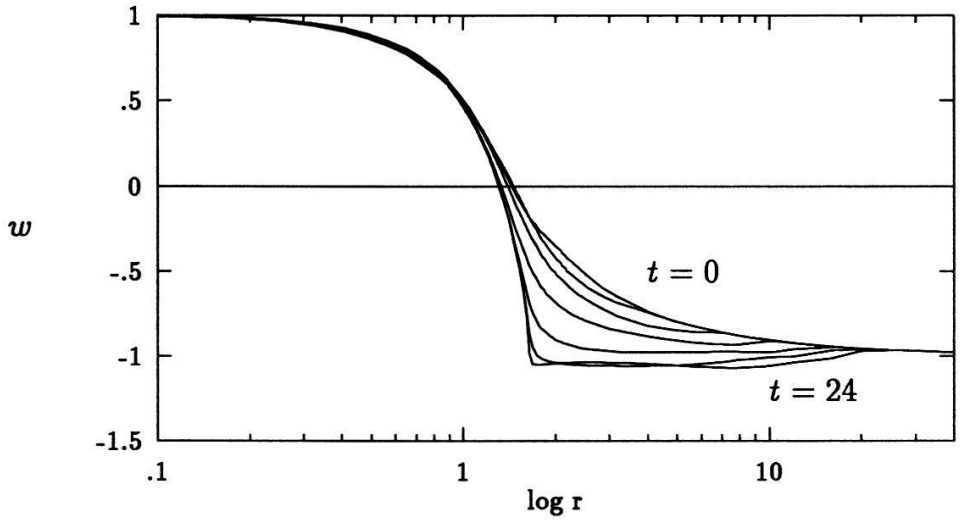

Figure 10a: The radial dependence of the YM amplitude w at various times in the interval $0 \leq t \leq 24$ for simulation I_1^-. Snapshots are taken in time intervals $\Delta t = 4$. The mini star collapses rapidly to a Schwarzschild black hole. For times $t > 24$ our numerical results are no more reliable.

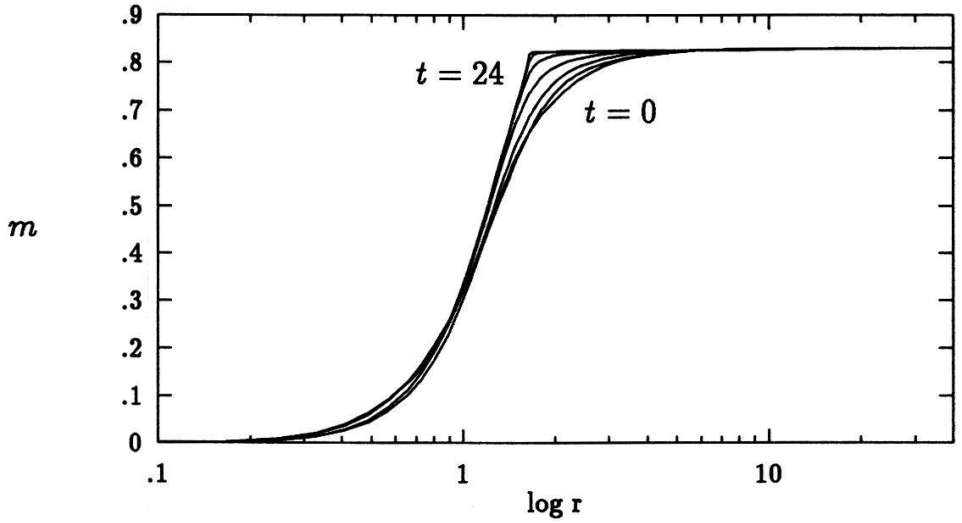

Figure 10b: The evolution of the metric variable m for the same parameters as in Fig.2a (simulation I_1^-). At $t = 24$ the star is already close to the Schwarzschild radius which corresponds to the total initial mass 0.8297. The latter is slightly bigger than the mass 0.8286 of the ground state BK solution.

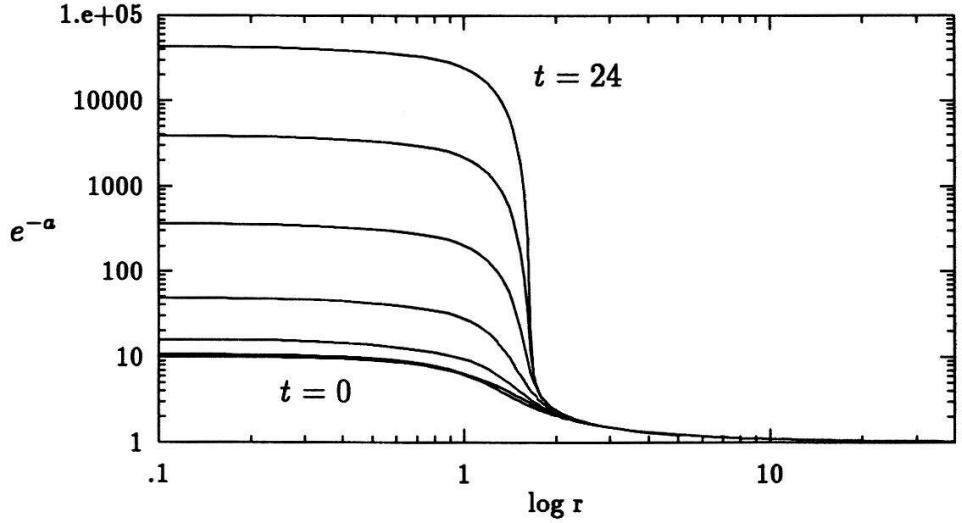

Figure 10c: The evolution of the inverse lapse function e^{-a} for simulation I_1^-. For $t = 24$ the lapse function is already smaller than 10^{-5}.

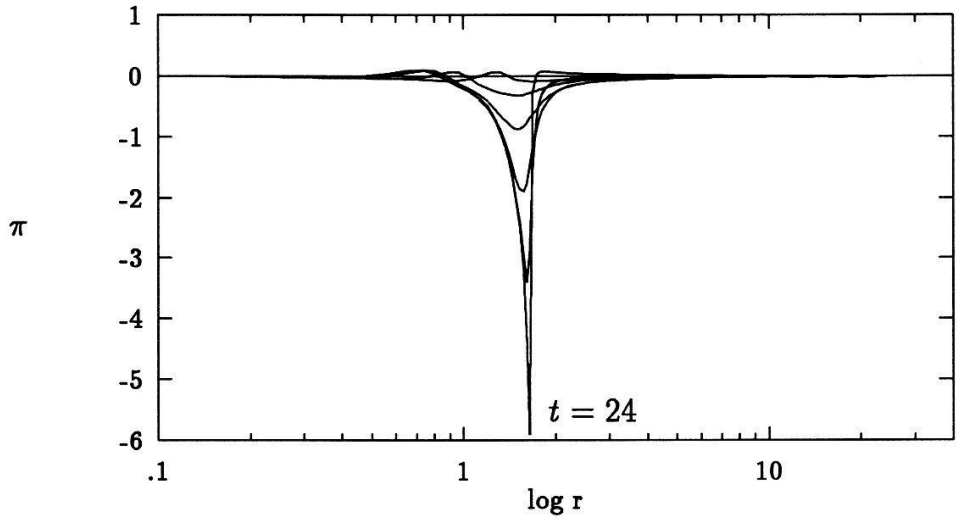

Figure 10d: The evolution of π, eqn.(41), for simulation I_1^- in the interval $0 \leq t \leq 24$.

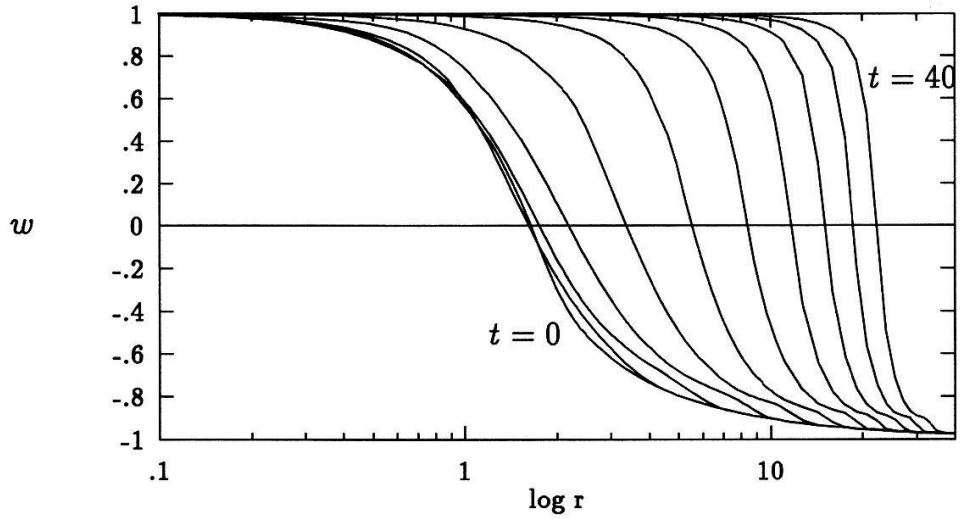

Figure 11a: Snapshots of the radial profiles of the YM amplitude for $0 \leq t \leq 40$ in time intervals $\Delta t = 4$ for simulation I_1^+. The mini star expands very rapidly. During the plotted time interval the outgoing motion has not yet reached the outer boundary of the grid.

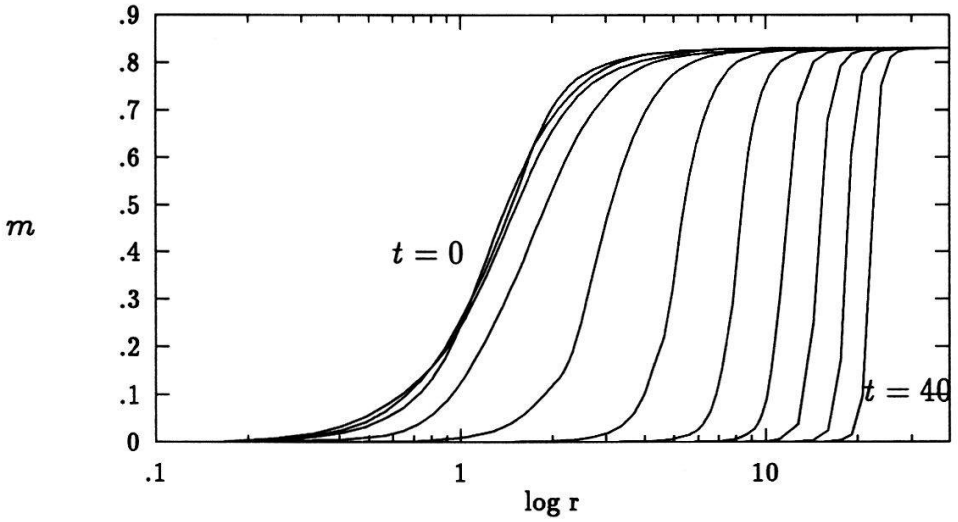

Figure 11b: Evolution of the mass variable m for simulation I_1^+. The 90% mass boundary moves outwards with about 3/4 of the speed of light.

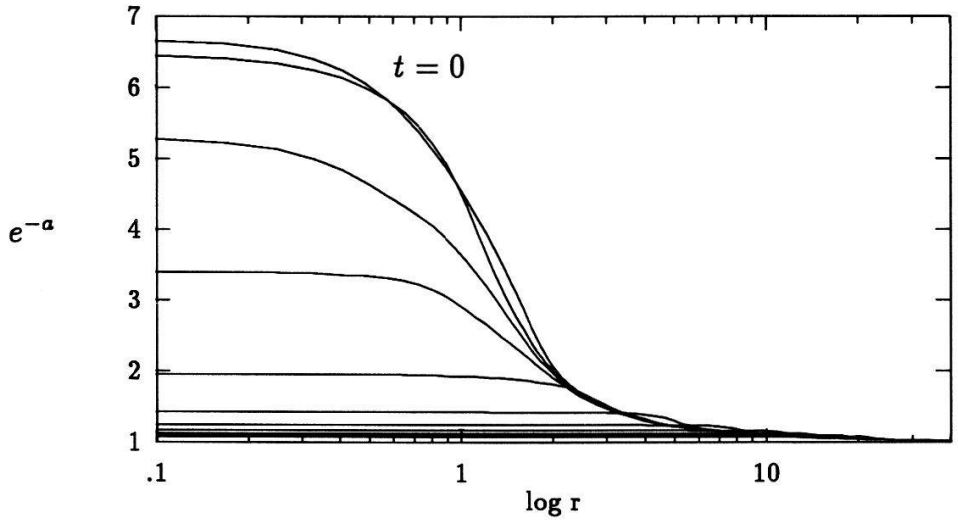

Figure 11c: Evolution of the inverse lapse function for simulation I_1^+.

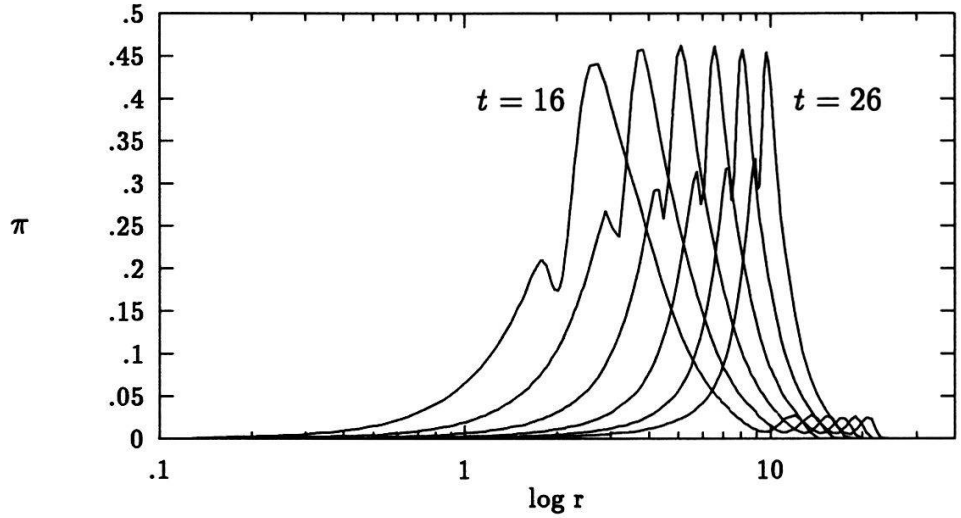

Figure 11d: Dynamical evolution of π (which is proportional to $\dot{w}$) for simulation I_1^+. The explosive character of the outward motion is clearly seen from this plot. The time increment of each peak is 2.

Fig.12 depicts the profile of w and m at $t = 0$ and $t = 24$ for the parameters I_2^-, II_1^-, II_2^-. The final results for the three simulations are so close that their difference is hardly visible in the figure. This fact reflects that at later times the behavior of the perturbed $SU(2)$ system is quite universal. This phenomenon also holds for the simulations I_2^+, II_1^+, II_2^+. Instead of collapse, these simulations lead to very similar explosions at later times, as can be seen from Figs.13a and 13b. These figures show the snapshots at $t = 0$ and $t = 40$.

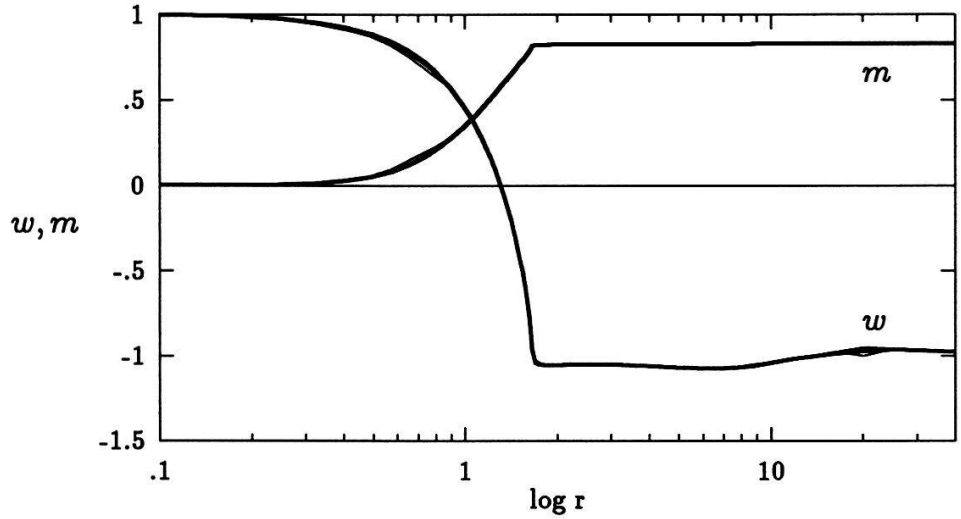

Figure 12: Profiles for w and m at $t = 24$ for the parameters I_2^- (thin line), II_1^- (bold line), and II_2^- (bold line).

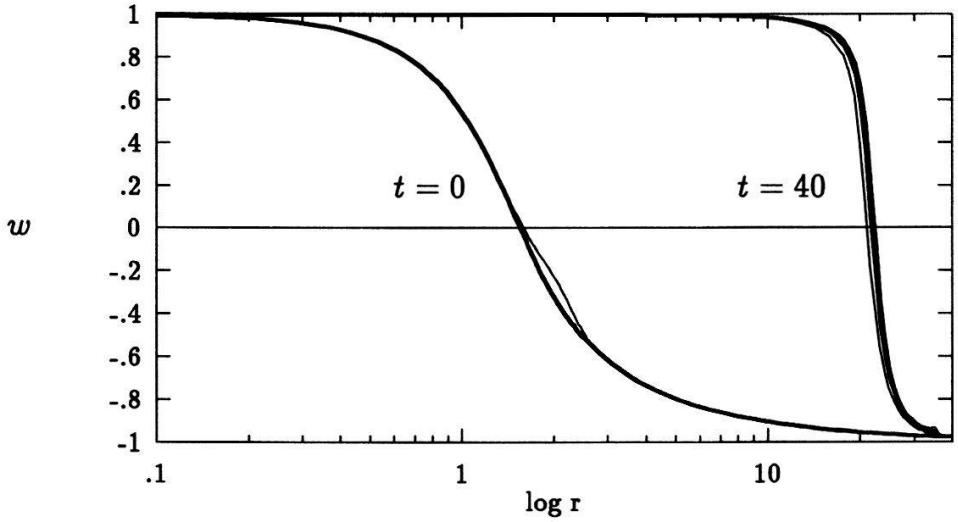

Figure 13a: Snapshots of the field amplitude w at times $t = 0$ and $t = 40$ for the parameters I_2^+ (thin line), II_1^+ (bold line), and II_2^+ (bold line). These three curves are so close together that their difference is hardly visible.

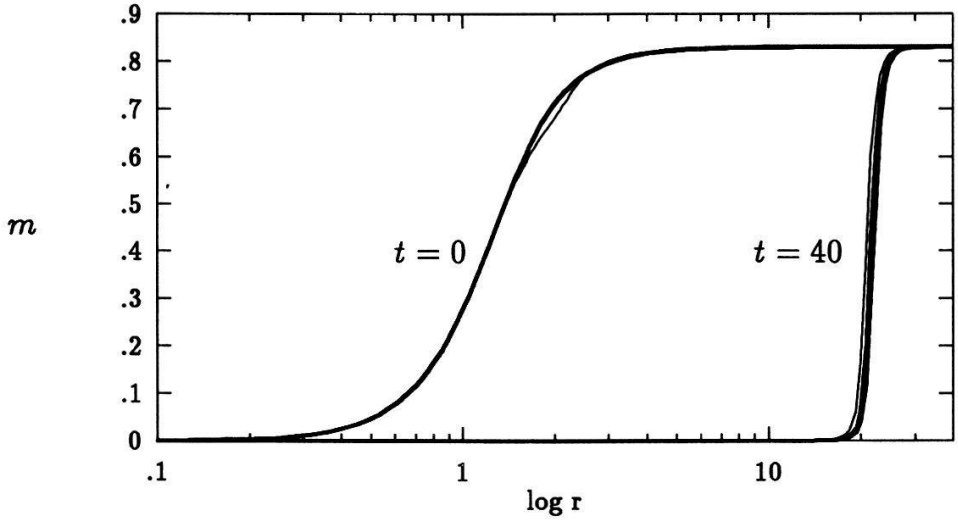

Figure 13b: Same as in Fig.5, but for the metric variable m.

In Fig.14, we compare the mass variable m at time $t = 24$ with that of the $k = 1$ colored black hole solution. We have chosen the horizon of the latter solution such that m at the horizon is equal to the formed black hole mass of the simulation I_1^-. The Fig.14 shows that the perturbed BK solution does not end up as a colored black hole but becomes a Schwarzschild black hole. This provides us evidence of the instability of colored black holes. On the other hand, as we discussed in section 3.3.3, the ground state BK solution is very

close to the exterior solution of the $k = 1$ black holes, at least for small 'size' black hole. This can be seen from the Fig.3 where we depict the BK ground state solution and the non-abelian back hole solution for $r_h = 0.2$. Therefore, we may regard the BK solution as a perturbation of non-abelian black hole solutions. The two types of representative simulations which we made can thus also be interpreted as the evolution of a perturbed black hole. The results of these simulations provide us further evidence that the colored black hole solutions are unstable indeed and have certain classes of perturbation evolve.

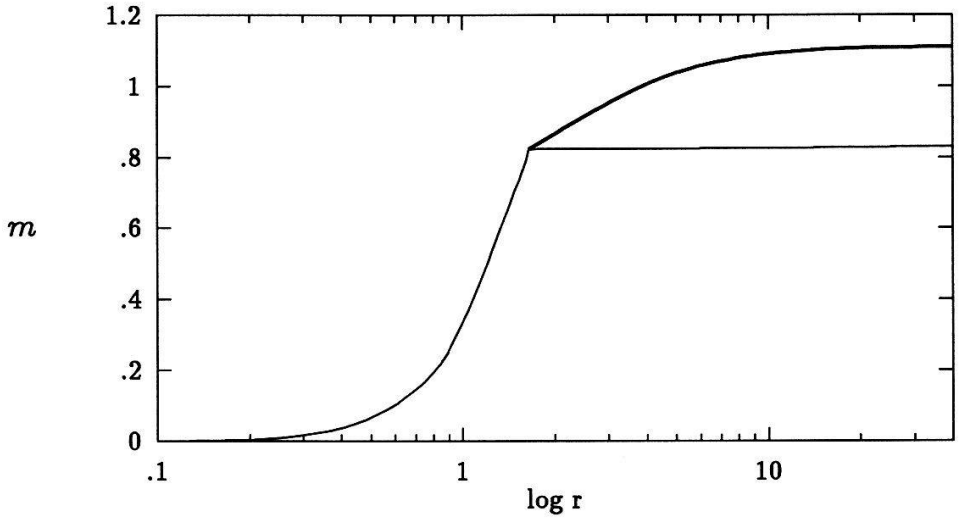

Figure 14: Profile of the mass variable m of Fig.10b at time $t = 24$ (thin line) and of the lowest energy colored black hole solution (bold line). The mass of the colored black hole at the horizon is chosen to be the same as that of the formed black hole for the simulation I_1^-.

6 Summary

In this paper, we have studied the stability of the remarkable BK and colored black hole solutions of the $SU(2)$ EYM system. For small radial perturbations, the frequency spectrum of the system is determined by a one-dimensional P-wave Schrödinger equation with a bounded potential. For both the BK and colored black hole solutions, it turns out that there exist bound states of this Schrödinger equation which correspond to exponentially growing modes. The BK solutions and the colored black holes are therefore linearly *unstable*, and they are also unstable in the sence of Liapunov.

The non-linear evolution of the perturbed EYM system has also been studied. We have investigated some representative perturbations of the 'ground state' BK solution. The non-linear evolution of these perturbations is in accordance with the conclusions of our linear stability analysis. Depending on the choice of the initial spherically symmetric perturbation, we found that either the YM repulsion dominates and the gauge boson star explodes, or gravity wins and the star collapse to a Schwarzschild black hole, but not to a colored black

hole. For a representative sample of perturbations, the late time behavior of the perturbed solutions is quite universal.

A systematic study of the dynamical evolution of the perturbed colored black holes is difficult because of the problems related with the event horizon. However, since the exterior solution of the colored black holes is very close to the BK solution, at least for small 'size' colored black holes, we may regard the BK solution as a perturbed black hole solution. Our simulations, therefore, can also be interpreted as the evolution of a class of black hole perturbations. The fact that the evolution does not end up as a colored black hole provides us further evidence of the instability of the colored black holes. Of course, in order to understand the behavior of the perturbed colored black holes comprehensively, we would need more sophisticated methods. We are working in this direction.

The BK solutions and the 'colored' black holes are very remarkable indeed, but they will never be found in reality because of their instability.

Acknowledgements

I would like to express my thanks to my supervisor Prof. Dr. N. Straumann for his invaluable guidance in the course of this work. Without his criticism, his suggestions and his patient reading of the draft, this work could not have been undertaken. To me, he is not only a supervisor but also an inspiring model as a scientist and as a personality.

My thanks also extend to the members and guests of the Institute for Theoretical Physics of the University of Zürich. In particular, I have benefited a lot from my discussions with G. Börner, T. Burwick, M. Heusler, Ph. Jetzer, C. Kiefer, D. Maison, L. O'Raifeartaigh and D. Wyler. I also wish to thank A. Aeppli and D. Bünzli for their help which facilitated the computer work .

Appendix

In Appendix A, we first give the $d+1$ splitting formalisms for the EYM system. Then, proofs of the Theorems 1 to 4 mentioned in the Introduction are given. The materials in this appendix is adapted from the ref. [50]. In Appendix B we present a flowchart for the program which we used to simulate the non-linear evolution of the perturbed equilibrium solutions of the $SU(2)$ EYM system.

A Static EYM Fields

A.1 The $d+1$ Splitting

Consider a static space-time (M, g). M is a direct product $M = R \times N$ and g can be chosen in the form

$$g = -\alpha^2 dt^2 + h, \tag{157}$$

where α is a non-negative function on N; t is the natural coordinate of R and ∂_t is the timelike Killing field corresponding to t. (N, h) is a 3-dimensional Riemanian space with a (time-independent) metric h. Here, we are not interested in black holes, and therefore assume that N is topologically an R^3.

Next, we split the source-free YM equations into space and time ($d+1$ splitting)[8]. Let

$$\begin{aligned} A &= A_i dx^i + A_0 dt \\ &\equiv \mathbf{A} + \phi dt, \end{aligned} \tag{158}$$

be the decomposition of the YM gauge potential. Throughout the Appendix A, the boldface letters always denote spatial objects. For the YM field strength we have then the decomposition

$$\begin{aligned} F &= dA + A \wedge A \\ &= \mathbf{dA} + \mathbf{A} \wedge \mathbf{A} + \mathbf{d}\phi \wedge dt + [\mathbf{A}, \phi] \wedge dt \\ &= \mathbf{F} + \mathbf{D}\phi \wedge dt \qquad (159) \\ &\equiv \mathbf{B} + \alpha \mathbf{E} \wedge dt, \qquad (160) \end{aligned}$$

where

$$\mathbf{B} = \mathbf{F} = \mathbf{dA} + \mathbf{A} \wedge \mathbf{A} \tag{161}$$

$$\alpha \mathbf{E} = \mathbf{D}\phi. \tag{162}$$

The homogeneous YM equation $DF = 0$ gives immediately

$$\begin{aligned} \mathbf{DB} &= 0, \\ \mathbf{D}(\alpha \mathbf{E}) + [\phi, \mathbf{B}] &= 0. \end{aligned} \tag{163}$$

For the Hodge-dual $*F$ we find the $d+1$ splitting

$$* F = \star \mathbf{E} - \alpha(\star \mathbf{B}) \wedge dt. \tag{164}$$

where $\star$ denotes the spatial Hodge-dual. Therefore, the YM equation $D * F = 0$ leads to the spatial equations

$$\begin{aligned} \mathbf{D} \star \mathbf{E} &= 0, \\ \mathbf{D}(\alpha \star \mathbf{B}) - [\phi, \star \mathbf{E}] &= 0. \end{aligned} \tag{165}$$

[8]This can be generalized easily to stationary situations by following the procedure in ref. [51].

Note that in the non-abelian case the static field equations for **E** and **B** do not decouple. We will use the general $d+1$ splitting formalisms established above in the next section. At this point we will show that the electric field **E** has to vanish for a regular solution under mild fall off assumptions at infinity.

Consider now a particlelike solution. Using the identity

$$Tr(\phi \mathbf{D} \star \mathbf{E}) = \mathbf{d}Tr(\phi \star \mathbf{E}) - Tr(\mathbf{D}\phi \wedge \star \mathbf{E}) \tag{166}$$

and (162) in the following consequence of (165)

$$\int_N Tr(\phi \mathbf{D} \star \mathbf{E}) = 0, \tag{167}$$

we obtain with the Stokes theorem

$$\int_N \alpha Tr(\mathbf{E} \wedge \star \mathbf{E}) = 0, \tag{168}$$

and hence $\mathbf{E} = 0$. The field equations (163) and (165) then reduce to the 'magnetostatic equations'

$$\begin{aligned} \mathbf{DB} &= 0, \\ \mathbf{D}(\alpha \star \mathbf{B}) &= 0. \end{aligned} \tag{169}$$

A.2 Non Existence Theorems

A.2.1 Non Existence of Static Einstein Solitons

Theorem: There exist no static gravitational solitons.

Proof: For the metric(157), the Einstein vacuum equations split as follows (see, eg. ref. [32])

$$\begin{aligned} \triangle \alpha &= 0, \\ \mathrm{Ric}(h) &= \tfrac{1}{\alpha}\mathrm{Hess}(\alpha). \end{aligned} \tag{170}$$

Using the maximum principle for harmonic functions and the asymptotic flatness condition

$$\alpha \to 1 \tag{171}$$

at spatial infinity, we obtain $\alpha \equiv 1$. Hence, $Ric(h) = 0$. In three dimensions this implies that the Riemann tensor vanishes and there remains only the trivial solution (Lichnerowicz[1]). □

Remark: If there is a event horizon, the previous argument does not work since the minimum of α is assumed on the horizon. However, the non-existence of gravitational solitons still holds (see [8, 9]); we do, however, not repeat the proof here.

A.2.2 Non Existence of Static YM Solitons

Theorem: Static YM solitons do not exist.

Proof: We recall Coleman's nice argument that there exist no particlelike solutions of the YM system in $d+1$ dimensions if $d \neq 4$ [3].

From (158) we find

$$(F,F) = (\mathbf{F},\mathbf{F}) + (\mathbf{D}\phi,\mathbf{D}\phi). \tag{172}$$

The r.h.s. of this equation is proportional to the Yang-Mills-Higgs Lagrangian without self-couplings in d dimensions. Thus we have

$$\begin{aligned} -\frac{1}{4}\int d^dx(F,F) & \\ = & -\frac{1}{4}\int d^dx((\mathbf{F},\mathbf{F}) - (\mathbf{D}\phi,\mathbf{D}\phi)) \\ = & S(\mathbf{A},\phi) \\ = & S_1 + S_2, \end{aligned} \tag{173}$$

where S_1 and S_2 are defined as follows

$$\begin{aligned} S_1 &= -\frac{1}{4}\int(\mathbf{F},\mathbf{F})d^dx, \\ S_2 &= \frac{1}{4}\int(\mathbf{D}\phi,\mathbf{D}\phi)d^dx. \end{aligned} \tag{174}$$

Since the energy of the soliton should be finite, both terms S_1 and S_2 have to be finite.

Suppose now that $(\mathbf{A}(\mathbf{x}),\phi(\mathbf{x}))$ is a solution to the system, i.e. $(\mathbf{A},\phi)$ is a critical point of the action S. We can embed this field configuration into the two-parameter family of variations

$$\phi(\mathbf{x};\sigma,\lambda) = \sigma\lambda\phi(\lambda\mathbf{x}), \tag{175}$$

$$\mathbf{A}(\mathbf{x};\sigma,\lambda) = \lambda\mathbf{A}(\lambda\mathbf{x}). \tag{176}$$

The action S thus has the following scaling behavior

$$S(\sigma,\lambda) = \sigma^2\lambda^{4-d}S_1 + \lambda^{4-d}S_2. \tag{177}$$

As $(\mathbf{A}(\mathbf{x}),\phi(\mathbf{x}))$ is a critical point of the action $S(\mathbf{A},\phi)$, it follows that

$$\frac{\partial}{\partial\sigma}S(\sigma,\lambda)\mid_{\sigma=\lambda=1}= 0, \tag{178}$$

$$\frac{\partial}{\partial\lambda}S(\sigma,\lambda)\mid_{\sigma=\lambda=1}= 0. \tag{179}$$

Hence, if $d \neq 4$, we find

$$S_1 = S_2 = 0. \tag{180}$$

Therefore,

$$\mathbf{F} = \mathbf{D}\phi = 0, \tag{181}$$

which implies $F = 0$ (for $d \neq 4$). The assumed solution $(\mathbf{A},\phi)$ are trivial only. □

A.2.3 Absence of Static EM Solitons

Theorem: There exist no Einstein-Maxwell solitons.

Proof: In the abelian case, we replace $\mathbf{D}$ in section A.1 by $\mathbf{d}$. Since the same argument in A.1 applies in the abelian case as well, we have $\mathbf{E} = 0$. It follows from (169) that $\mathbf{d}(\alpha \star \mathbf{B}) = 0$. Hence, we can repeat the arguments from (166) to (168) – with replacement of $\mathbf{E}$ by $\star\mathbf{B}$ – we find also $\mathbf{B} = 0$. The EM system thus reduces to the vacuum case and no non-trivial solutions exist.□

A.2.4 Absence of Static EYM Solitons in 2+1 Dimensions

Theorem: There exist no static EYM solitons in 2+1 dimensions.

Proof: We have proved $\mathbf{E} = 0$ in A.1. However, the reasoning for $\mathbf{B} = 0$ in (A.2.3) can not be generalized to the non-abelian case. As first remarked by Deser [2], the non-trivial solutions in $2+1$ dimensions can be easily excluded. Indeed, $\omega := \alpha \star \mathbf{B}$ is a space-time scalar for $d = 2$. From $\mathbf{D}\omega = 0$, we obtain for the norm $|\omega|$ of ω (in group space) the condition

$$\mathbf{d}|\omega| = 0, \tag{182}$$

which implies for $d = 2$ that $|\omega| = const.$ This constant must vanish, otherwise there would be a $\mathbf{B}$ field which does not vanish asymptotically. The EYM system in $D = 2 + 1$ thus reduces again to the vacuum case and no non-trivial solutions exist. □

B Flowchart of the Program

In this appendix, we present a brief flowchart of the program used for simulating non-linear evolutions of the perturbed equilibrium solutions of the EYM system. The RK solver in the flowchart includes a routine of the 4th order Runge-Kutta method and routines of the cubic-spline interpolation provided by the E01BAF and E02BBF from the NAG library. The routines E01BAF and E02BBF interpolate midpoints between grid points so that the 4th order Runge-Kutta method can be used. The Predictor and Corrector are routines for the modified MacCormack algorithm, in which 4-point difference formulae for the first order derivative are used. Second order derivatives are centered differenced. For a detailed description, see Section 5.1. The routine Hamiltonian constraint performs as an accuracy monitor. The program was written in FORTRAN and run on an Alliant machine.

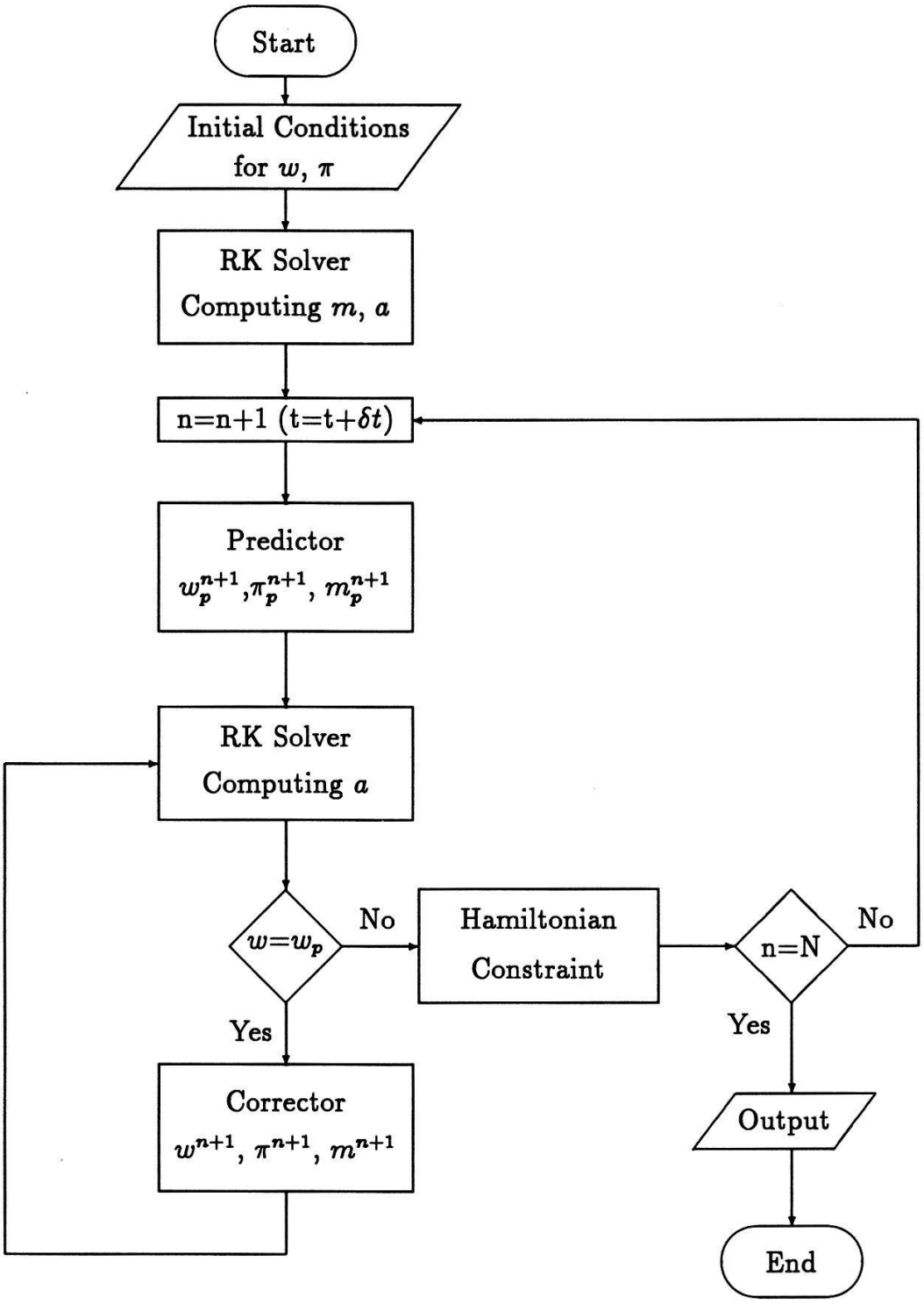
Start
Initial Conditions for w, π
RK Solver Computing m, a
n=n+1 (t=t+δt)
Predictor w_p^{n+1}, π_p^{n+1}, m_p^{n+1}
RK Solver Computing a
$w=w_p$
No
Hamiltonian Constraint
n=N
No
Yes
Yes
Corrector w^{n+1}, π^{n+1}, m^{n+1}
Output
End

References

[1] A. Lichnerowicz, in *Théories relativistes de la gravitation et de l'éléctromagnetisme* (Masson, Paris, 1955).

[2] S. Deser, Phys. Lett. **B64** (1976) 463.

[3] S. Coleman, in *New Phenomenon in Subnuclear Physics*, ed. A. Zichichi (Plenum, New York, 1975).

[4] S. Deser, Class. Quantum Grav. **1** (1984) L1.

[5] A. A. Ershov and D. V. Gal'tsov, Phys. Lett. **A150** (1990) 159.

[6] E. Malec, Acta Phys. Polon. **B15** (1984) 1101;
E. Malec, Acta Phys. Polon. **B18** (1987) 1017.

[7] R. Bartnik and J. McKinnon, Phys. Rev. Lett. **61** (1988) 141.

[8] W. Israel, Commun. Math. Phys. **8** (1968) 245.

[9] D. Robinson, Gen. Rela. Grav. **8** (1977) 695.

[10] G. Bunting and A. Masood-ul-Alam, Gen. Rela. Grav. **19** (1987) 147.

[11] B. Carter, in *Gravitation in Astrophysics*, ed. by B. Carter and J. B. Hartle (Plenum, New York 1987).

[12] M. Perry, Phys. Lett. **B71** (1977) 234.

[13] P. B. Yasskin, Phys. Rev. **D12** (1975) 2212.

[14] D. V. Gal'tsov and A. A. Ershov, Phys. Lett. **A138** (1989) 160.

[15] M. S. Volkov and D. V. Galt'sov, Sov. Pisma ZETF **50** (1989) 312; JETP Lett. **50** (1990) 346.

[16] M. S. Volkov and D. V. Gal'tsov, Sov. J. Nucl. Phys. **51** (1990) 747.

[17] H. P Künzle and A. K. M. Masood-ul-Alam, J. Math. Phys. **31**(4) (1990) 928.

[18] P. Bizon, Phys. Rev. Lett. **64** (1990) 2844.

[19] J. A. Smoller, A. G. Wasserman, S. T. Yau and J. B. McLeod, Commun. Math. Phys. **143** (1991) 115.

[20] M. Heusler and N. Straumann, MPA preprint, MPA 634 (1991); Zürich University preprint ZU-TH29/91.

[21] N. Straumann and Z. H. Zhou, Phys. Lett. **B237** (1990) 353.

[22] N. Straumann and Z. H. Zhou, Phys. Lett. **B243** (1990) 33.

[23] P. Bizon, Phys. Lett. **B259** (1991) 53.

[24] P. Bizon and R. M. Wald, Phys. Lett. **B267** (1991) 173.

[25] D. V. Galt'sov and M. S. Volkov, to appear in Phys. Lett. A.

[26] Z. H. Zhou and N. Straumann, Nuclear Physics, **B360** (1991) 180.

[27] H. P. Künzle, Alberta University Preprint, (1991).

[28] D. V. Galt'sov and M. S. Volkov, Crete University preprint, (1991).

[29] S. Droz. M. Heusler and N. Straumann, Phys. Lett. **B268** (1991) 371.

[30] M. Heusler, S. Droz and N. Straumann, Phys. Lett. **B271** (1991) 61.

[31] M. Heusler, S. Droz and N. Straumann, private communication.

[32] N. Straumann, *General Relativity and Relativistic Astrophysics* (Springer, Berlin, 1985).

[33] H. C. Wang, *On invariant connections over a principal fibre bundle*, Nagoya Math. J. **13** (1958) 1;
S. Kobayashi and K. Nomizu, *Foundations of differential geometry*, vol.1, (John Wiley & Sons, New York, 1963).
J. Harnad, S. Shnuider and L. Vinet, J. Math. Phys. **21** (1980) 2179.

[34] O. Brodbeck and N. Straumann, to be published.

[35] P. Forgács and N. S. Manton, Commun. Math. Phys. **72** (1980) 15.

[36] E. Witten, Phys. Rev. Lett. **38** (1977) 121.

[37] P. Bizon and O. T. Popp, Universität Wien preprint, UWThPh-1991-20.

[38] H. Boutaleb-Joutei, A. Chakrabarti and A. Comtet, Phys. Rev. D **20** (1979) 1884.

[39] B. Harrison et.al., *Gravitation Theory and Gravitational Collapse*, (The University of Chicago Press, Cambridge, 1965).

[40] V. Bargmann, Proc. Natl. Acad. Sci. USA **38** (1952) 961.

[41] F. Calogero, *Variable Phase Approach to Potential Scattering*, (Academic Press, New York and London, 1967).

[42] D. Maison, private communication.

[43] C. Hirsch, *Numerical Computation of Internal and External Flows*, Vol. 2, (John Wiley & Sons, 1990).

[44] D. H. Bernstein, D. W. Hobill and L. L. Smarr, in *Frontiers in Numerical Relativity*, edited by C. R. Evans et.al., (Cambridge University Press, 1989).

[45] E. Seidel and W. M. Suen, Phys. Rev. **D42** (1990) 384.

[46] S. Koonin and D. C. Meredith, *Computational Physics*, (Addison-Wesley Publishing Company, 1990).

[47] R. Durrer, M. Heusler, P. Jetzer and N. Straumann, Phys. Lett., **B259** (1991) 48.

[48] N. Turok and D. Spergel, Phys. Rev. Lett., **64** (1990) 2736.

[49] R. Durrer, M. Heusler, P. Jetzer and N. Straumann, Zürich University Preprint, ZU-TH9/91 (1991), to appear in Nucl. Phys B.

[50] N. Straumann, Bad Honnef Lectures (1991), to be published.

[51] R. Durrer and N. Straumann, Helv. Phys. Acta, **61** (1988) 1027.